NASA TECHNICAL NOTE

NASA TN D-5004

c. 1

NASA TN D-5004

ROUGHNESS DRAG DUE TO TWO-DIMENSIONAL FABRICATION-TYPE SURFACE ROUGHNESS ON AN OGIVE CYLINDER FROM FORCE TESTS AT TRANSONIC SPEEDS

by K. R. Czarnecki and William J. Monta

Langley Research Center
Langley Station, Hampton, Va.

NATIONAL AERONAUTICS AND SPACE ADMINISTRATION • WASHINGTON, D. C. • JANUARY 1969

ROUGHNESS DRAG DUE TO TWO-DIMENSIONAL FABRICATION-TYPE SURFACE ROUGHNESS ON AN OGIVE CYLINDER FROM FORCE TESTS AT TRANSONIC SPEEDS

By K. R. Czarnecki and William J. Monta

Langley Research Center
Langley Station, Hampton, Va.

NATIONAL AERONAUTICS AND SPACE ADMINISTRATION

For sale by the Clearinghouse for Federal Scientific and Technical Information
Springfield, Virginia 22151 – CFSTI price $3.00

ROUGHNESS DRAG DUE TO TWO-DIMENSIONAL FABRICATION-TYPE SURFACE ROUGHNESS ON AN OGIVE CYLINDER FROM FORCE TESTS AT TRANSONIC SPEEDS

By K. R. Czarnecki and William J. Monta
Langley Research Center

SUMMARY

An investigation has been made in the transonic Mach number range from 0.70 to 1.20 and over a range of free-stream Reynolds number per foot from about 0.8×10^6 to 6.0×10^6 (2.6×10^6 to 19.7×10^6 per meter) to determine by means of force tests the roughness drag due to essentially two-dimensional fabrication-type surface roughness immersed in a turbulent boundary layer. Six types of surface roughness, including step, wave, crease, and swept configurations, were investigated. The tests were made on an ogive cylinder of fineness ratio 12.2, the roughness elements covering the cylindrical portion of the models. Some force-test data obtained previously on these models at Mach numbers of 1.61 and 2.01 have been included as an aid to the analysis, and a comparison is made of the force-test results with those results obtained from the pressure-distribution investigations and with supersonic wave-drag theory.

The investigation indicated that roughness elements submerged in a turbulent boundary layer had drag characteristics very much like those of bodies in a uniform free stream as the Mach number was increased or the roughness sweep angle was changed. There was, however, a strong influence of change in Reynolds number or boundary-layer thickness (by inference) on the drag characteristics when substantial wave drag was present. In general, the agreement between the drag data obtained from force tests and pressure tests was good. Roughness drag was apparently primarily pressure drag at both subsonic and supersonic Mach numbers. Agreement between supersonic theory and experiment tended to improve as Mach number and unit Reynolds number were increased, but would apparently tend to be degraded if the Reynolds number were to be increased merely by increasing model length. Sweeping the roughness element delayed the tendency toward agreement between theory and experiment toward higher Mach numbers. Because of low unit Reynolds numbers in flight and the desire to build smooth-surface aircraft, a good knowledge of boundary-layer effects on roughness drag will be required for the proper estimation of roughness drag.

INTRODUCTION

As part of a program to provide design information for supersonic aircraft, a general investigation is being made at the Langley Research Center to determine the drag of fabrication-type surface roughness in a turbulent boundary layer. Various techniques, including model force tests, roughness-element surface pressure distributions, boundary-layer profile surveys, and schlieren photography, are being utilized in this research. The tests are being conducted in a variety of facilities and over a wide range of operating conditions. Some of the results obtained in this investigation have been presented in references 1 to 5.

Analysis of the aforementioned results disclosed that at supersonic speeds, the greatest component of drag due to surface roughness in a turbulent boundary layer is pressure or wave drag. (See refs. 4 and 5.) Theoretical considerations further indicated that this wave drag would be greatest and subject to the most complex Mach-number—boundary-layer interactions near sonic velocity. Consequently, it was deemed desirable to extend the investigation to turbulent boundary layers in the transonic-flow regime. The basic longitudinal pressure distributions and schlieren photographs obtained in these transonic-flow tests have been presented in reference 6 and the integrated pressure drags, in reference 7. Some additional comments were made on the pressure distributions in reference 8. This paper presents the results of force-test measurements at transonic speeds to obtain roughness-drag coefficients and relates the drag results with those obtained from force tests on the same models at Mach numbers of 1.61 and 2.01 (ref. 3 and unpublished data). A comparison is made of the force-test results with those obtained from the pressure-distribution investigations and also, where appropriate, with supersonic theory.

The force tests were made on six types of fabrication roughness built into the cylindrical portion of an ogive cylinder with a fineness ratio of 12.2 and on a smooth-surface reference model. The tests were made over a Mach number range from 0.70 to 1.20 and over a range of free-stream Reynolds number per foot from about 0.8×10^6 to 6.0×10^6 (2.6×10^6 to 19.7×10^6 per meter). The model axis was always alined with the free stream, and turbulent boundary-layer flow was assured by means of a carborundum-grain trip near the tip of the model nose.

SYMBOLS

Measurements for this investigation were taken in the U.S. Customary Units but are also given parenthetically in the International System of Units (SI). (See ref. 9.)

$C_{D,p}$ roughness-element pressure-drag coefficient based on model wetted area,

$$\frac{\pi}{S_w}\int_{r^2_{min}}^{r^2_{max}}\left[(C_p)_{ff} - (C_p)_{rf}\right]dr^2 \times \text{Number of roughness elements}$$

$C_{D,s}$ free-stream coefficient of surface drag (skin-friction drag plus roughness pressure drag), $\frac{D_{total} - D_{nose} - D_{base}}{q_\infty S_w}$

$\Delta C_{D,s}$ increment between free-stream surface-drag coefficients for rough and smooth bodies under same test conditions, $(C_{D,s})_{rough} - (C_{D,s})_{smooth}$

C_F average skin-friction drag coefficient for smooth body, $(C_{D,s})_{smooth}$

C_p pressure coefficient, $\frac{p_l - p_\infty}{q_\infty}$

D_{base} pressure drag of base

D_{nose} pressure drag of nose

D_{total} drag of model as indicated by balance, including skin-friction and pressure drags

M Mach number

p static pressure

p_t free-stream stagnation pressure

q dynamic pressure, $0.7pM^2$

R radius of ogive

R/ft (R/m) free-stream Reynolds number per foot (per meter) or unit Reynolds number

R_L Reynolds number based on free-stream flow conditions and model length

r local model radius measured normal to body axis

S	surface area of complete model, including nose
x	axial distance from tip of model nose
γ	ratio of specific heats
δ	estimated total boundary-layer thickness

Subscripts:

f	based on frontal area
w	based on wetted surface area
ff	forward-facing surface
rf	rearward-facing surface
l	local conditions just outside boundary layer
∞	free stream
max	maximum
min	minimum

APPARATUS AND METHODS

Wind Tunnel

This investigation was conducted in the Langley 8-foot transonic pressure tunnel, which is a single-return closed-circuit pressure tunnel, capable of operating at stagnation pressures from 0.25 to 2 atmospheres. The Mach number in the slotted test section, which is square, can be continuously varied from 0 to 1.20. The Mach number distribution without a model is reasonably uniform throughout the test-section length of about 5 feet (1.52 meters), with the maximum deviation from the average free-stream Mach number being on the order of ± 0.005 at the subsonic Mach numbers to ± 0.02 at the highest test Mach numbers (ref. 10).

Models and Instrumentation

An ogive cylinder 50.0 inches (127.0 cm) long and 4.096 inches (10.40 cm) in diameter with a 3-caliber nose was the basic configuration of the eight sting-mounted models tested. Two models were plain or essentially smooth ogive cylinders without roughness elements. (See fig. 1.) The remaining six models were smooth on the ogive sections, but each had a number of cycles of a particular fabrication roughness constructed into the whole length of the cylindrical portion of the body. (See figs. 2 and 3.) These roughness cycles included steps with grooves, rearward-facing steps, creases, and protruding waves, each having a nearly constant cycle length of from 1.5 to 4.0 inches (3.8 to 10.2 cm) and a constant height of from 0.014 to 0.053 inch (0.036 to 0.135 cm). The heights of the various roughness elements were selected to represent fabrication imperfections found on recent production transonic aircraft of aluminum construction, and the cycle lengths were chosen to provide enough cycles on the models (table I) so that a measurable difference in drag would be obtainable in the force tests. On four of these models, the roughness cycles were wrapped around the model unswept; on the remaining two, they were swept 45°. The relationship of the maximum roughness height to the estimated total boundary-layer thickness (by the method of ref. 11) is shown in figure 4 for $M_{\infty} = 1.00$. There was little change for the other Mach numbers.

One of the plain ogive cylinders, which was used to establish nose drag values (see table II for orifice locations), was constructed of aluminum. The remaining models, including the smooth-body reference-drag model, were made of wood covered with Paraplex and fiber glass. The first 2 inches (5.08 cm) of the nose of each of the ogive cylinders with fabrication roughness was aluminum in order to minimize tip damage.

The surface finish of all force models was very smooth, usually less than 10 microinches (0.25 μm). Small-scale waviness was often present on the models, superimposed on some of the roughness cycles. Although this condition prevented all cycles on any model from being identical, the deviations from the desired contours were generally few enough and small enough to have no influence upon the conclusions drawn from these tests.

The six rough-skin models of this investigation are the same models for which pressure distributions were determined in reference 6. The pressure orifices were sealed and the external pressure tubing was cut off so the same bodies could be tested as balance models without the need for making tare corrections.

A six-component internal strain-gage balance was used to measure model forces. Two interchangeable axial-force drag beams of 30 lbf (135 N) and 60 lbf (270 N) were used to cover the test range. Three precision automatic-indicating manometers were provided to measure tunnel reference pressures and model-base pressure.

Test Methods

All tests were made at an angle of incidence of 0° with a fully turbulent boundary layer, transition being promoted by No. 60 carborundum grains cemented to the model 0.75 inch (1.9 cm) from the tip. The base plug, of the same diameter as the model, was located 1/16 inch (0.16 cm) behind the model, as indicated in figure 1. It was used in all tests to reduce the balance axial force and to help maintain uniform pressure over the model base. Data were obtained with the tunnel conditions being held in equilibrium. During all runs, the dewpoint temperature was maintained low enough to prevent condensation effects.

Range of Tests

Tests were made on each model at Mach numbers of 0.70, 0.90, 1.00, 1.10, and 1.20. Data were taken at nominal stagnation pressures of 500, 1000, 1500, 2000, 2500, and 3000 psf absolute (23 900, 47 900, 71 800, 95 800, 119 800, and 143 600 N/m^2). The Reynolds numbers per foot corresponding to these pressures vary with Mach number and range from about 0.8×10^6 to 5.0×10^6 (2.6×10^6 to 16.4×10^6 per meter) at $M_\infty = 0.70$ and from about 1.0×10^6 to 6.0×10^6 (3.3×10^6 to 19.7×10^6 per meter) at $M_\infty = 1.20$. Stagnation temperature was maintained at a value of $120^{\circ} \pm 2^{\circ}$ F ($322^{\circ} \pm 1^{\circ}$ K) throughout the tests.

RESULTS AND DISCUSSION

Flow Conditions on Smooth Reference Model

The basic flow conditions existing on the smooth-surface reference model can be deduced from the axial pressure distributions determined for the model and presented in figure 5. A solid line has been faired through the average data at each Mach number. The approximate locations of the stations at which pressure distributions have been determined over the roughness elements are shown by the braces.

The basic pressure distributions have been discussed in reference 7. The main objective in presenting these data is to indicate that the forward-station roughness elements are generally located in a regime of more adverse pressure gradient and of higher local Mach number (more negative pressure coefficient), as well as in a thinner boundary layer (fig. 4) than the rearward-station roughness elements, and that there is shock impingement (of the reflected nose shock) on the cylindrical portion of the model at the low supersonic Mach numbers ($M_\infty = 1.1$ and 1.2) and a recompression shock on the cylinder at $M_\infty = 1.0$ (x = 24 in. or 61 cm). Thus, there is a diversity of local flow conditions influencing the drag characteristics of each of the individual roughness elements which contribute to the total roughness drag perceived by the balance. Some of these local flow

effects, such as those due to the reflected nose shocks, will not correspond to those that can be expected in free flight. However, these departures are not believed to be serious enough to affect the overall trends for the wind-tunnel and free-flight flow regimes.

Skin-Friction Drag of Smooth Reference Model

The skin-friction drag of the smooth reference model is presented in figure 6. The experimental results are compared with turbulent-boundary-layer theoretical values for a smooth flat plate computed by the T' method of Sommer and Short (ref. 12). This theoretical approach usually provides good agreement with flat-plate results obtained in the Mach number range of these tests.

The experimental results for the smooth reference body fall somewhat below the theoretical curves. Because of the presence of the ogival nose on the body, which is not accounted for in the theory, the expectation was that experiment would be slightly higher than theory. One possible explanation for this discrepancy could be that the nose pressure distributions measured on the aluminum model may not correspond exactly to those existing on the smooth reference body (or, for that matter, on any of the roughness models). The experimental results indicate a decreasing skin-friction drag level with increasing Mach number, as predicted by theory. There is some scatter in the data in terms of both changing Reynolds number and changing Mach number, but this scatter appears to be within the limitations imposed by the estimated accuracies of the pressure and force measurements.

Drags of Models With Surface Roughness

The surface drags of the models with roughness are presented in figure 7. For simplicity, the experimental data are compared with the theoretical range of flat-plate skin-friction drag rather than with the more numerous and more scattered experimental smooth-body skin-friction drag results of figure 6. The objective of this figure is merely to show the type of roughness data obtained; the analysis of the roughness effects can be performed more conveniently in terms of incremental drags due to surface roughness.

Incremental Drags Due to Surface Roughness

The incremental drags due to surface roughness are presented in figure 8. These increments were determined by finding the difference in drag between the individual drag coefficients for the rough model and smooth curves faired through the smooth-reference-body skin-friction data parallel to skin-friction theory. This procedure reduced the random scatter considerably below that obtained by using the reference-body data points directly. The largest increments in drag were incurred by the 0.053-inch (0.135-cm) protruding waves (fig. 8(b)) and the smallest increments, by the 0.014-inch (0.036-cm)

45° creases (fig. 8(f)). The effects of changes in Reynolds number and Mach number were dependent upon the type of roughness configuration involved.

For the 0.021-inch (0.053-cm) steps with grooves (fig. 8(a)), the drag data tended to cluster around two faired curves: one for the subsonic Mach numbers and another higher one for the transonic and supersonic Mach numbers. Within these Mach number regimes, there was little effect of Mach number. As the model Reynolds number R_L was increased, the magnitude of the incremental drag coefficients increased, but at a decelerating rate at the higher Reynolds numbers.

For the 0.053-inch (0.135-cm) wave and crease models (figs. 8(b) and 8(c)), increasing the Mach number increased $\Delta C_{D,s}$ over the complete test Mach number range. The rate of increase was, of course, greater at the transonic and supersonic speeds because of incurrence of wave drag (ref. 8). At subsonic speeds, the effects of Reynolds number were relatively small. At sonic and supersonic speeds, however, increasing R_L rapidly increased $\Delta C_{D,s}$, but again at a decelerating rate at the higher Reynolds numbers.

The incremental drag coefficients for the 0.017-inch (0.043-cm) transverse creases (fig. 8(d)) were considerably smaller than for the larger wave and crease roughnesses. Furthermore, the Reynolds number effects tended to be rather unrecognizable because of the relatively high inaccuracy associated with the small coefficients involved, particularly at the lower values of R_L.

Of the sweptback roughness configurations (figs. 8(e) and 8(f)), the 0.020-inch (0.051-cm) 45° rearward steps had the higher drag. The drag increments of the swept-crease model were apparently nearly within the accuracy of the data. Again, the relatively large scatter in the data at low values of R_L is readily discernible.

Comparison of Drag Results From Force and Pressure Tests

In figures 9 and 10, the incremental surface-drag data from the force tests are plotted as functions of both Reynolds number and free-stream Mach number and are compared with the drag results obtained from pressure tests (ref. 7). The single horizontal bar corresponds to the drag level that would exist if each element had a drag equal to the drag of an element at the forward pressure-test station (figs. 1 and 5). The double horizontal bar similarly corresponds to the drag level that would exist if each roughness element had a drag equal to that determined from the pressure-distribution tests for an element at the rearward test station. In addition, in figure 10, a comparison is made between experimental force-test drag and theoretical pressure drag for the supersonic free-stream Mach numbers.

In general, the agreement between the drag data obtained from force tests and pressure tests regarding overall drag levels, Reynolds number effects, and Mach number

effects was good. In figures 10(a) to 10(c), increasing the force-test results by a constant coefficient value over the Mach number range for the models represented would have made the agreement excellent. This observation suggests that there may be an error creeping into the force-test data from some undetermined source which is constant over the Mach number range. The most significant conclusion to be made is that roughness elements submerged in a turbulent boundary layer have drag characteristics very much like those of bodies in a uniform free stream as the Mach number is increased or the roughness sweep angle is changed. There was, however, a strong influence of change in Reynolds number or boundary-layer thickness (by inference) when substantial wave drag was present. There was a disagreement between results from force tests and pressure tests for the model with 0.053-inch (0.135-cm) transverse creases (fig. 10(c)) at $M_\infty = 1.61$ and 2.01. This discrepancy was due to the inadequate distribution of orifices in these earlier pressure tests at these Mach numbers, which led to too high integrated pressure coefficients. Inasmuch as the pressure-drag coefficients do not include boundary-layer friction, the indicated conclusion is that roughness drag was primarily pressure drag, even at subsonic Mach numbers. That roughness drag was primarily pressure drag at supersonic speeds has already been indicated by the boundary-layer survey tests reported in reference 5.

Comparison of Force- and Pressure-Test Results With Supersonic Theory

The supersonic theory presented in figure 10 by means of dashed curves is based on the assumption that the average wave-drag coefficient for all the roughness elements on any model is equal to the average of the theoretical wave-drag coefficients for the elements at stations 1 and 2 as computed in reference 7 but referenced to model wetted surface area. Roughness-element sweepback effects were computed by the standard normal-component procedure. For the model with 0.021-inch (0.053-cm) steps with grooves, the arbitrary assumption was made that the theoretical drag coefficient could be expressed by the equation

$$C_{D,p} = \frac{2}{\gamma M_\infty{}^2} \frac{S_f}{S_w}$$

A similarly arbitrary curve allowing for sweepback effects was assumed for the model having 0.020-inch (0.051-cm) 45° rearward steps.

The results of figure 10 indicate that as the free-stream Mach number was increased, theory tended toward better agreement with experiment. As the Reynolds number was increased by increasing the unit Reynolds number (i.e., by increasing the tunnel stagnation pressure), the agreement between theory and experiment tended to improve at the supersonic test Mach numbers. Analysis of the pressure distributions at $M_\infty = 1.61$ and 2.01 for the models with wave- and crease-type roughness (ref. 4) indicates that at

these speeds, the disagreement between theory and experiment, which is still considerable, was almost entirely due to the presence of the boundary layer. (The surface slopes were much too small for significant nonlinear effects to be present, and the method of characteristics gave results practically identical to linear theory.) Consequently, the deduction can be made that if the Reynolds number is increased by increasing the model length while maintaining the roughness height constant, the effect will be to degrade the agreement between theory and experiment. This result is to be expected because the more rearward roughness elements will be immersed in a progressively thicker boundary layer where the damping or interaction effects will be stronger. Furthermore, note should be taken that a supersonic transport, for example, will fly at unit Reynolds numbers of 2×10^6 per foot (6.6×10^6 per meter) or less, which correspond to the test conditions at the lower tunnel stagnation pressures where the boundary-layer effects are most powerful. Also, on actual airplanes, attempts will be made to keep the roughness as small as possible, and thus the ratio of boundary-layer thickness to roughness height will be increased still further. Obviously, then, a good knowledge of boundary-layer effects on roughness drag will be required for the proper estimation of roughness drag.

The data for the models with unswept 0.053-inch (0.135-cm) roughness (figs. 10(b) and 10(c)) show that the experimental results for the model with creases fell considerably more below theory than those for the model with protruding waves. This result is ascribed to the fact that the inner recesses of the creases were filled with dead air, which acted as a cushion and prevented this part of the crease from affecting the more exterior flow.

The results for the 0.020-inch (0.051-cm) 45° rearward steps (fig. 10(e)) indicate that the maximum incremental surface-drag coefficient occurred shortly after the free-stream Mach line had crossed over the swept roughness element. For the 0.014-inch (0.036-cm) 45° creases (fig. 10(f)), it appears that the maximum coefficient may occur when the Mach line lies somewhat farther behind the line of the roughness element, although it should be noted that the incremental-drag accuracy for this configuration is relatively low. For both cases, agreement between theory and experiment was delayed toward higher free-stream Mach numbers by the effects of sweep.

SUMMARY OF RESULTS

An investigation has been made in the transonic Mach number range from 0.70 to 1.20 and over a range of free-stream Reynolds number per foot from about 0.8×10^6 to 6.0×10^6 (2.6×10^6 to 19.7×10^6 per meter) to determine by means of force tests the roughness drag due to essentially two-dimensional fabrication-type surface roughness immersed in a turbulent boundary layer. The force-test results at transonic speeds were compared with those obtained at Mach numbers of 1.61 and 2.01, with results obtained

from related pressure-distribution investigations, and with supersonic wave-drag theory. The investigation indicates the following conclusions:

Roughness elements submerged in a turbulent boundary layer have drag characteristics very much like those of bodies in a uniform free stream as the Mach number is increased or the roughness sweep angle is changed.

There was, however, a strong influence of change in Reynolds number or boundary-layer thickness (by inference) on the drag characteristics when substantial wave drag was present.

In general, the agreement between the drag data obtained from force tests and pressure tests was good.

Roughness drag is apparently primarily pressure drag at both subsonic and supersonic Mach numbers.

Agreement between supersonic theory and experiment tended to improve as Mach number and unit Reynolds number were increased, but would apparently tend to be degraded if the Reynolds number were to be increased merely by increasing model length.

Sweeping the roughness element delayed the tendency toward agreement between theory and experiment toward higher free-stream Mach numbers.

Because of low unit Reynolds numbers in flight and the desire to build smooth-surface aircraft, a good knowledge of boundary-layer effects on roughness drag will be required for the proper estimation of roughness drag.

Langley Research Center,
National Aeronautics and Space Administration,
Langley Station, Hampton, Va., October 28, 1968,
126-13-02-11-23.

REFERENCES

1. Czarnecki, K. R.; Robinson, Ross B.; and Hilton, John H., Jr.: Investigation of Distributed Surface Roughness on a Body of Revolution at a Mach Number of 1.61. NACA TN 3230, 1954.

2. Sevier, John R.; and Czarnecki, K. R.: Investigation of Effects of Distributed Surface Roughness on a Turbulent Boundary Layer Over a Body of Revolution at a Mach Number of 2.01. NACA TN 4183, 1958.

3. Czarnecki, K. R.; Sevier, John R., Jr.; and Carmel, Melvin M.: Effects of Fabrication-Type Roughness on Turbulent Skin Friction at Supersonic Speeds. NACA TN 4299, 1958.

4. Czarnecki, K. R.; and Monta, William J.: Pressure Distributions and Wave Drag Due to Two-Dimensional Fabrication-Type Surface Roughness on an Ogive Cylinder at Mach Numbers of 1.61 and 2.01. NASA TN D-835, 1961.

5. Czarnecki, K. R.; and Monta, William J.: Boundary-Layer Velocity Profiles and Skin Friction Due to Surface Roughness on an Ogive Cylinder at Mach Numbers of 1.61 and 2.01. NASA TN D-2048, 1963.

6. Czarnecki, K. R.; and Monta, William J.: Pressure Distributions Due to Two-Dimensional Fabrication-Type Surface Roughness on an Ogive Cylinder at Transonic Speeds. NASA TN D-3516, 1966.

7. Czarnecki, K. R.; and Monta, William J.: Pressure Drags Due to Two-Dimensional Fabrication-Type Surface Roughness on an Ogive Cylinder at Transonic Speeds. NASA TN D-3519, 1966.

8. Czarnecki, K. R.: The Problem of Roughness Drag at Supersonic Speeds. NASA TN D-3589, 1966.

9. Mechtly, E. A.: The International System of Units – Physical Constants and Conversion Factors. NASA SP-7012, 1964.

10. Mugler, John P., Jr.: Transonic Wind-Tunnel Investigation of the Aerodynamic Loading Characteristics of a 60° Delta Wing in the Presence of a Body With and Without Indentation. NACA RM L55G11, 1955.

11. Tucker, Maurice: Approximate Calculation of Turbulent Boundary-Layer Development in Compressible Flow. NACA TN 2337, 1951.

12. Sommer, Simon C.; and Short, Barbara J.: Free-Flight Measurements of Turbulent Boundary-Layer Skin Friction in the Presence of Severe Aerodynamic Heating at Mach Numbers From 2.8 to 7.0. NACA TN 3391, 1955.

TABLE I.- MODEL DESIGNATIONS

Model	Designation	Number of cycles of roughness
1	Smooth	--------
2	0.021-inch (0.053-cm) steps with grooves	9
3	0.053-inch (0.135-cm) protruding waves	24
4	0.053-inch (0.135-cm) transverse creases	24
5	0.017-inch (0.043-cm) transverse creases	24
6	0.020-inch (0.051-cm) 45^{o} rearward steps	5 stripes
7	0.014-inch (0.036-cm) 45^{o} creases	6 stripes

TABLE II.- ORIFICE LOCATIONS FOR MODEL 1

Orifice	Axial distance from tip of model nose	
	in.	cm
1	1.01	2.57
2	1.95	4.95
3	2.82	7.16
4	3.81	9.68
5	4.78	12.14
6	5.78	14.68
7	6.76	17.17
8	7.76	19.71
9	8.77	22.28
10	9.79	24.87
11	10.78	27.38
12	11.80	29.97
13	12.78	32.46
14	13.77	34.98
15	14.78	37.54
16	15.78	40.08
17	16.78	42.62
18	17.75	45.09
19	18.79	47.73
20	19.78	50.24
21	20.78	52.78
22	22.75	57.78
23	24.74	62.84
24	26.77	68.00
25	28.76	73.05
26	30.77	78.16
27	32.76	83.21
28	34.78	88.34
29	36.79	93.45
30	42.14	107.04
31	44.10	112.01
32	46.08	117.04
33	48.08	122.12
34	49.62	126.03

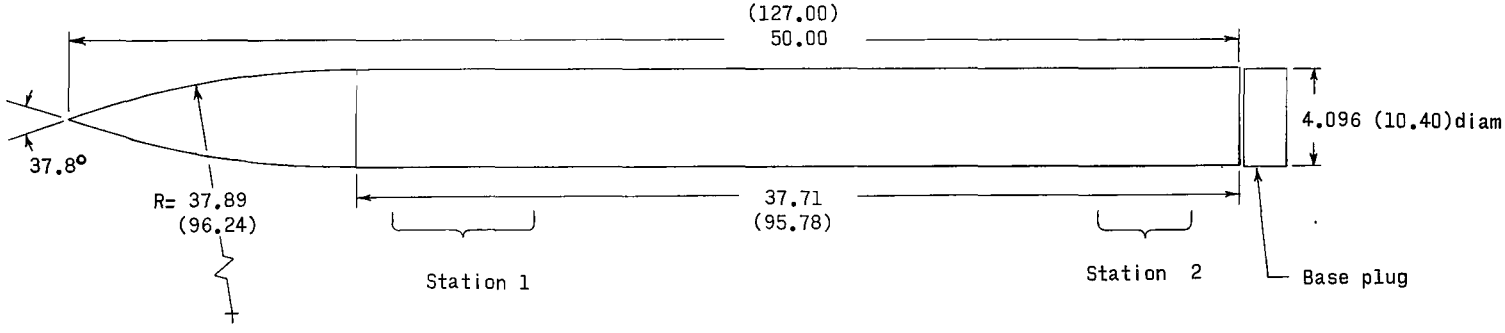

Figure 1.- Sketch of basic model. All dimensions are in inches (centimeters in parentheses) unless otherwise stated.

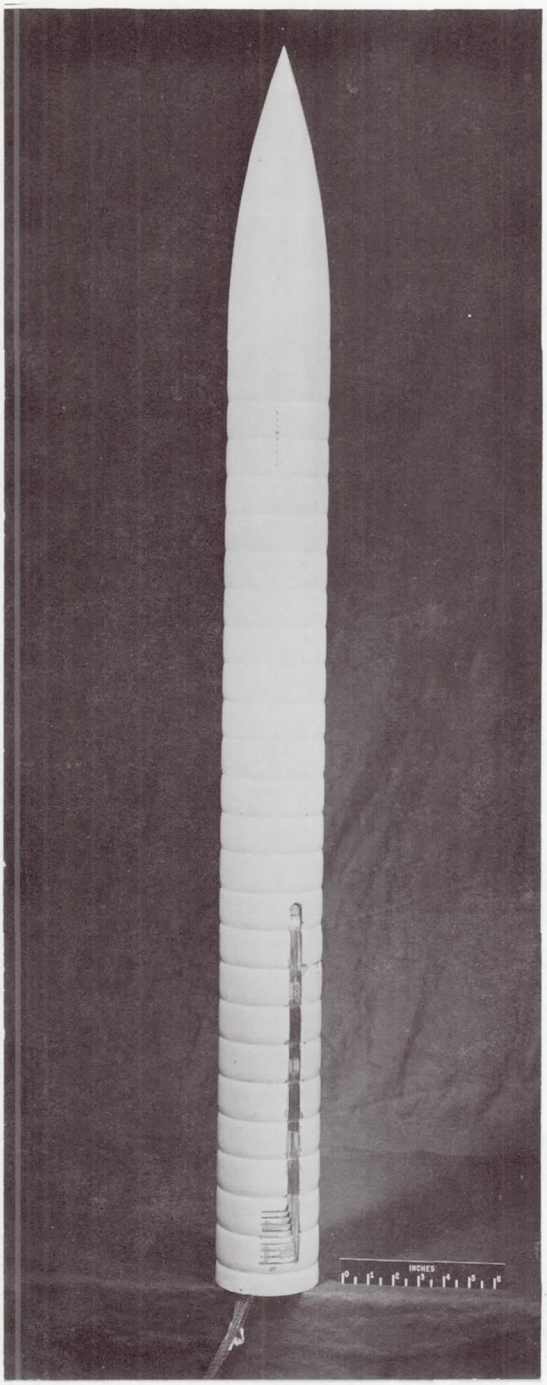

(a) 0.053-inch (0.135-cm) transverse creases.

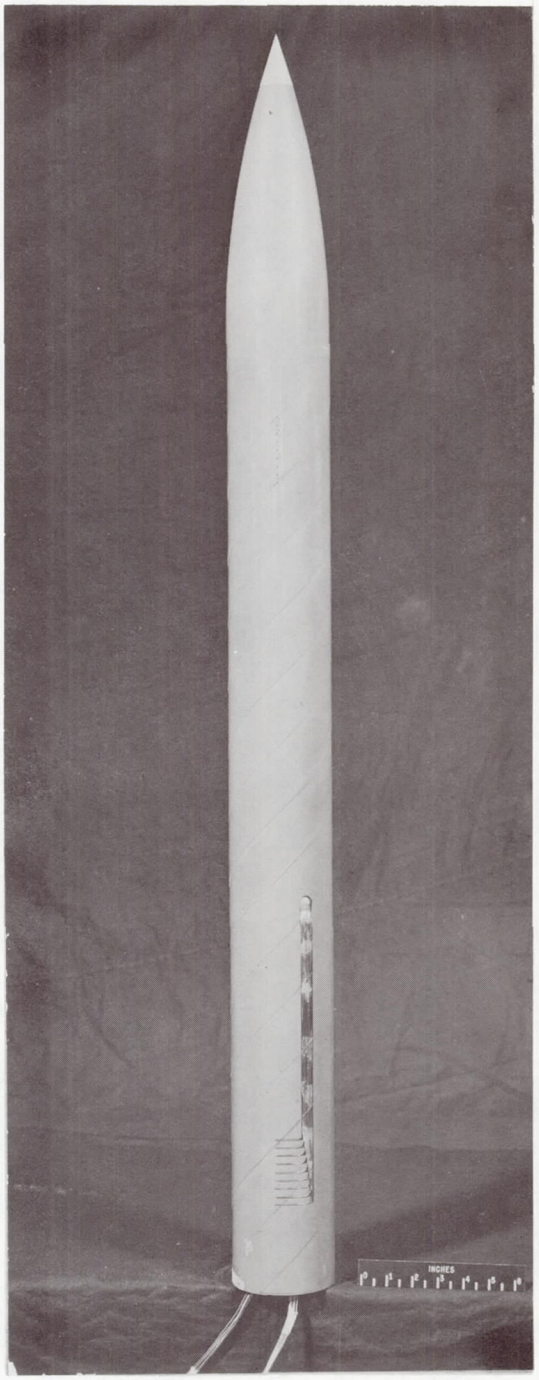

(b) 0.020-inch (0.051-cm) 45° rearward steps.

Figure 2.- Photographs of typical roughness models. L-61-1039

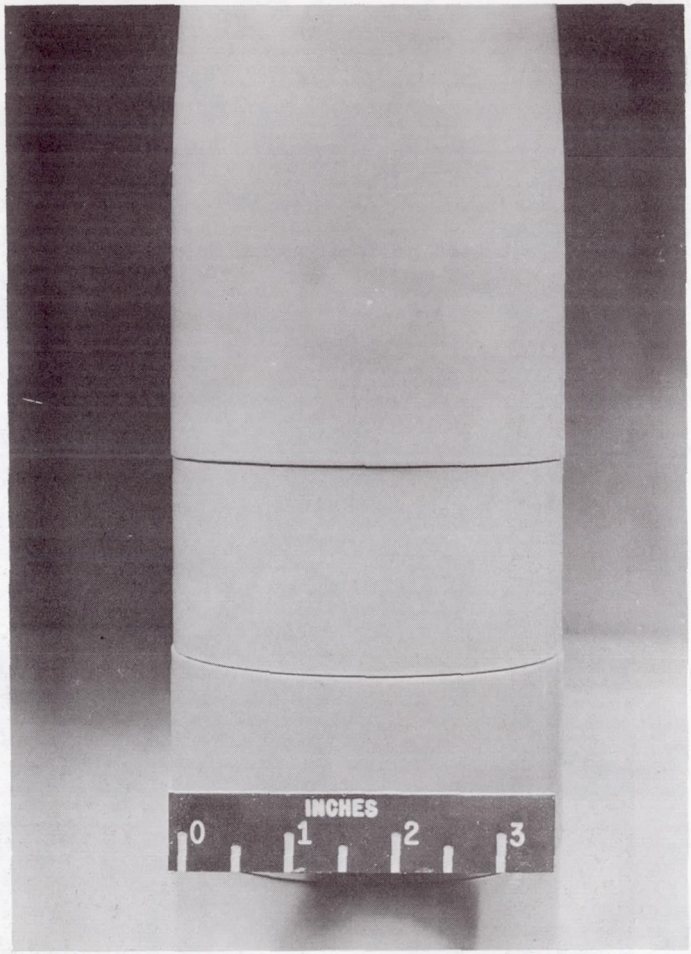

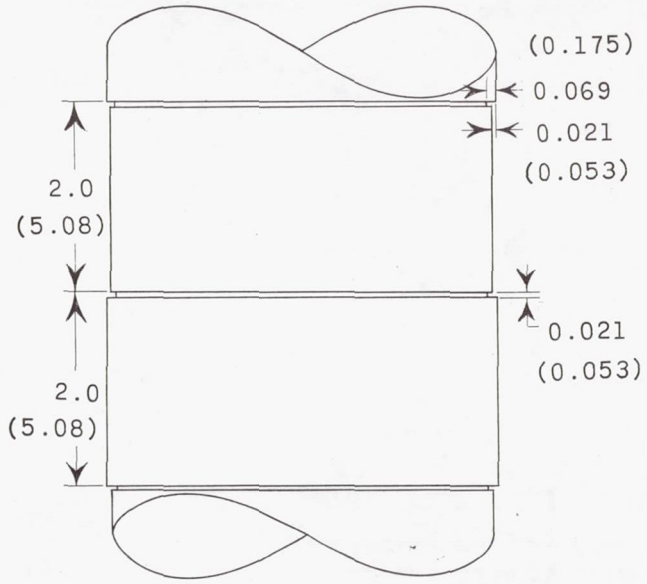

(a) 0.021-inch (0.053-cm) steps with grooves. L-61-1040

Figure 3.- Details of fabrication-type roughness. All dimensions are in inches (centimeters in parentheses) unless otherwise stated.

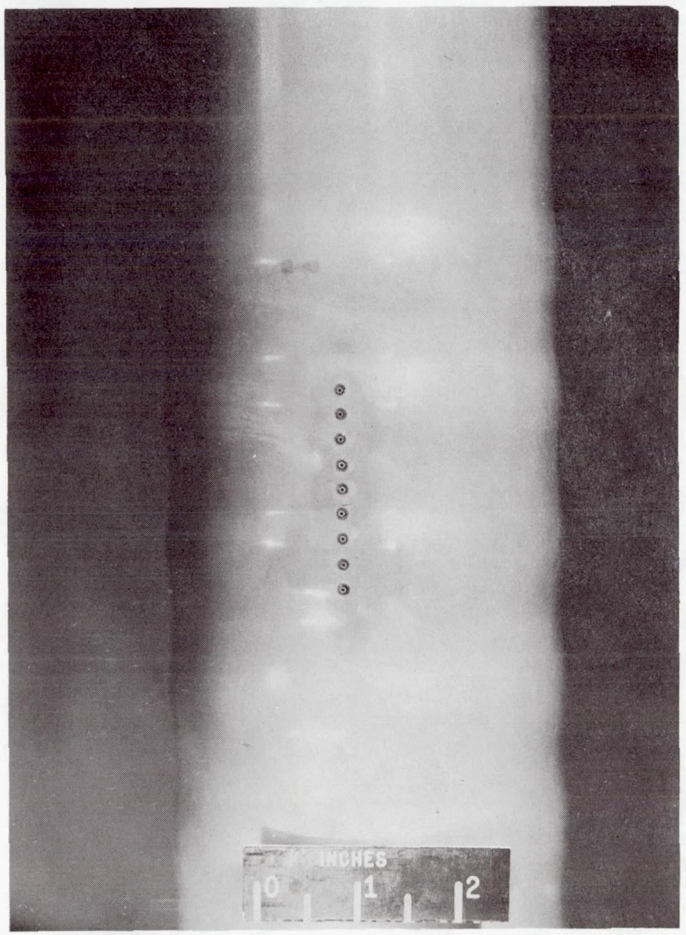

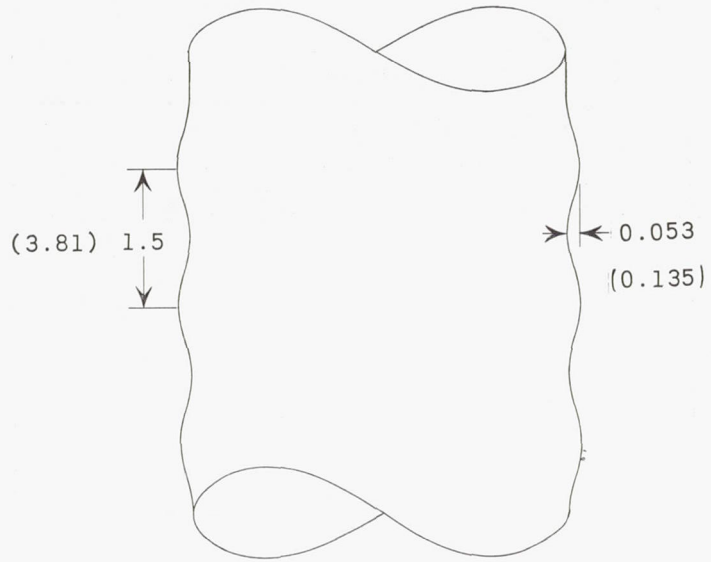

(b) 0.053-inch (0.135-cm) protruding waves. L-61-1043

Figure 3.- Continued.

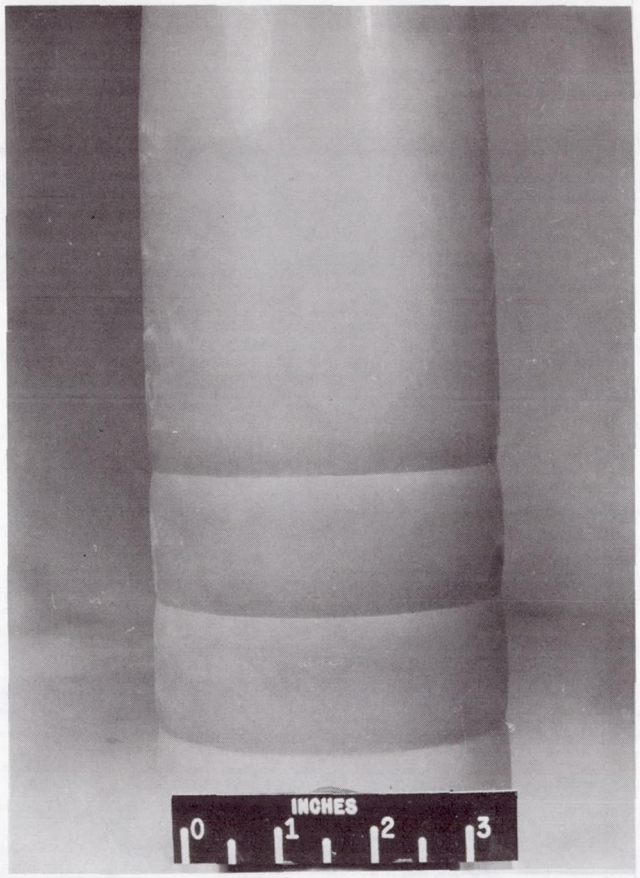

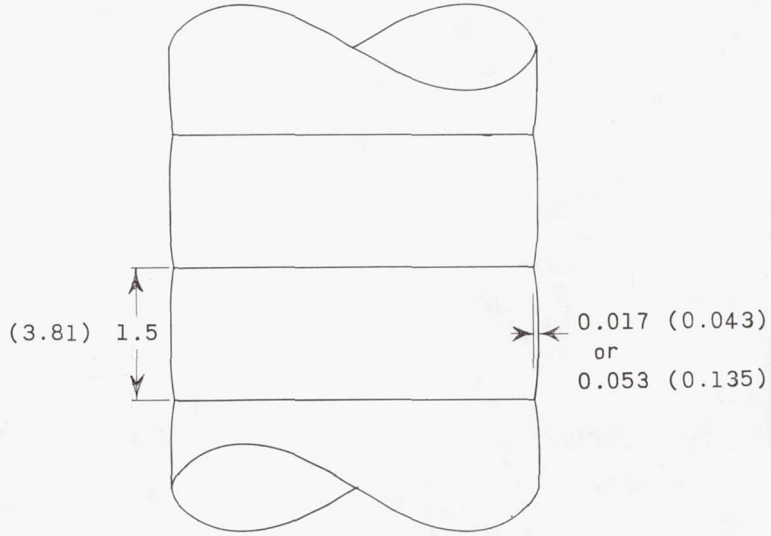

(c) 0.017-inch (0.043-cm) and 0.053-inch (0.135-cm) transverse creases.

Figure 3.- Continued.

L-61-1044

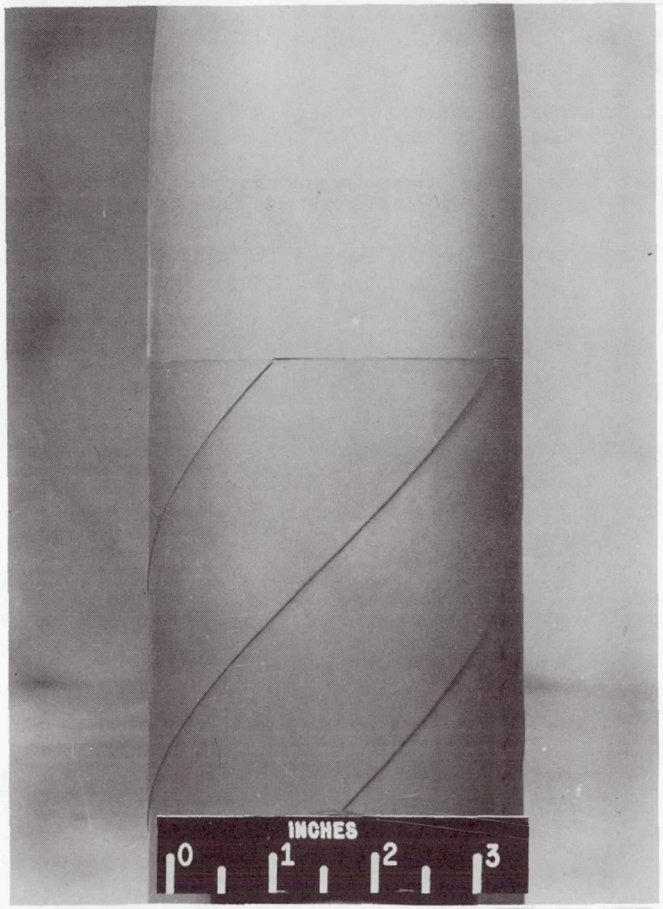

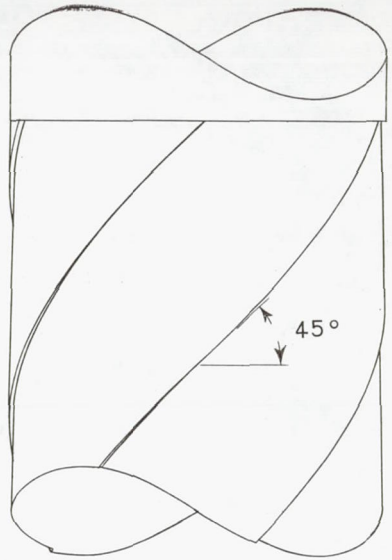

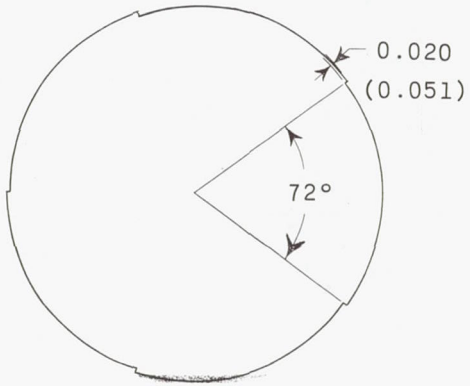

(d) 0.020-inch (0.051-cm) 45^{0} rearward steps.

Figure 3.- Continued.

L-61-1045

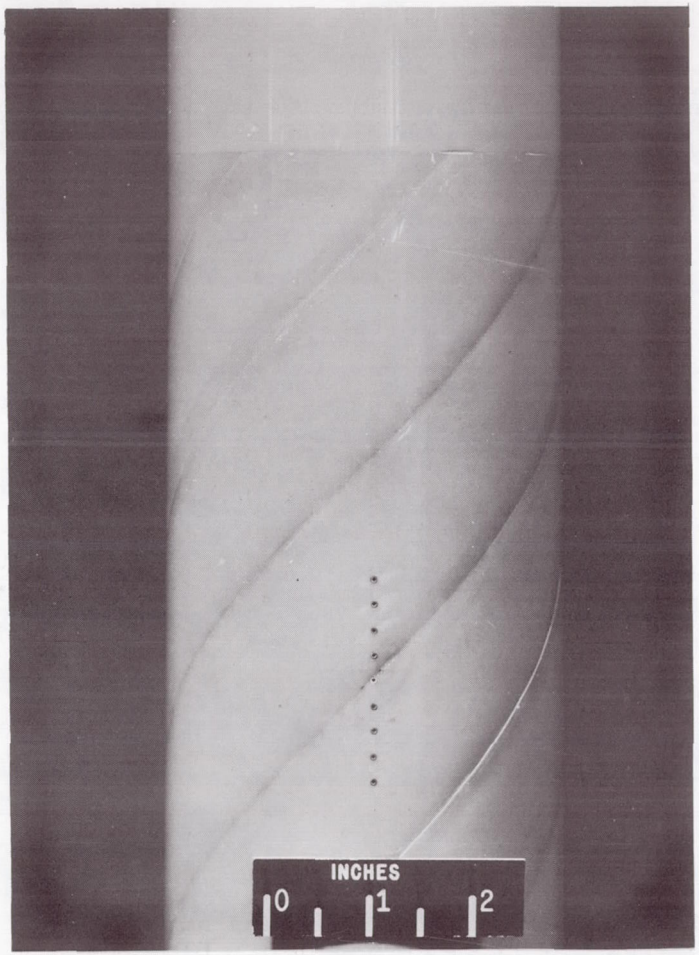

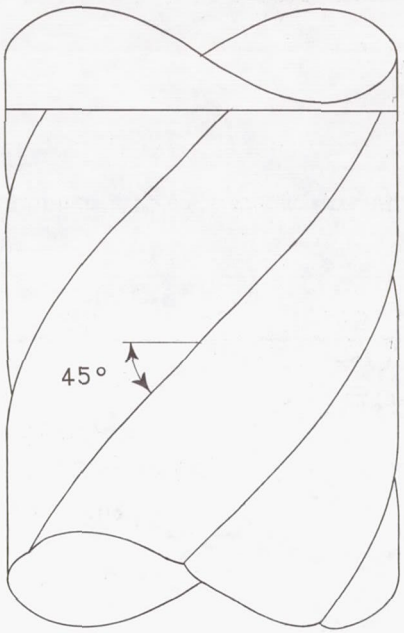

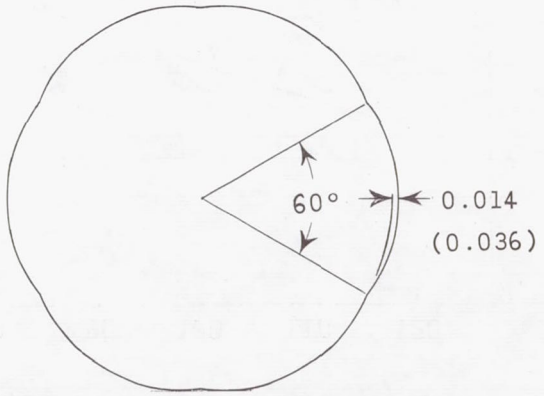

(e) 0.014-inch (0.036-cm) 45^{0} creases.

Figure 3.- Concluded.

L-61-1046

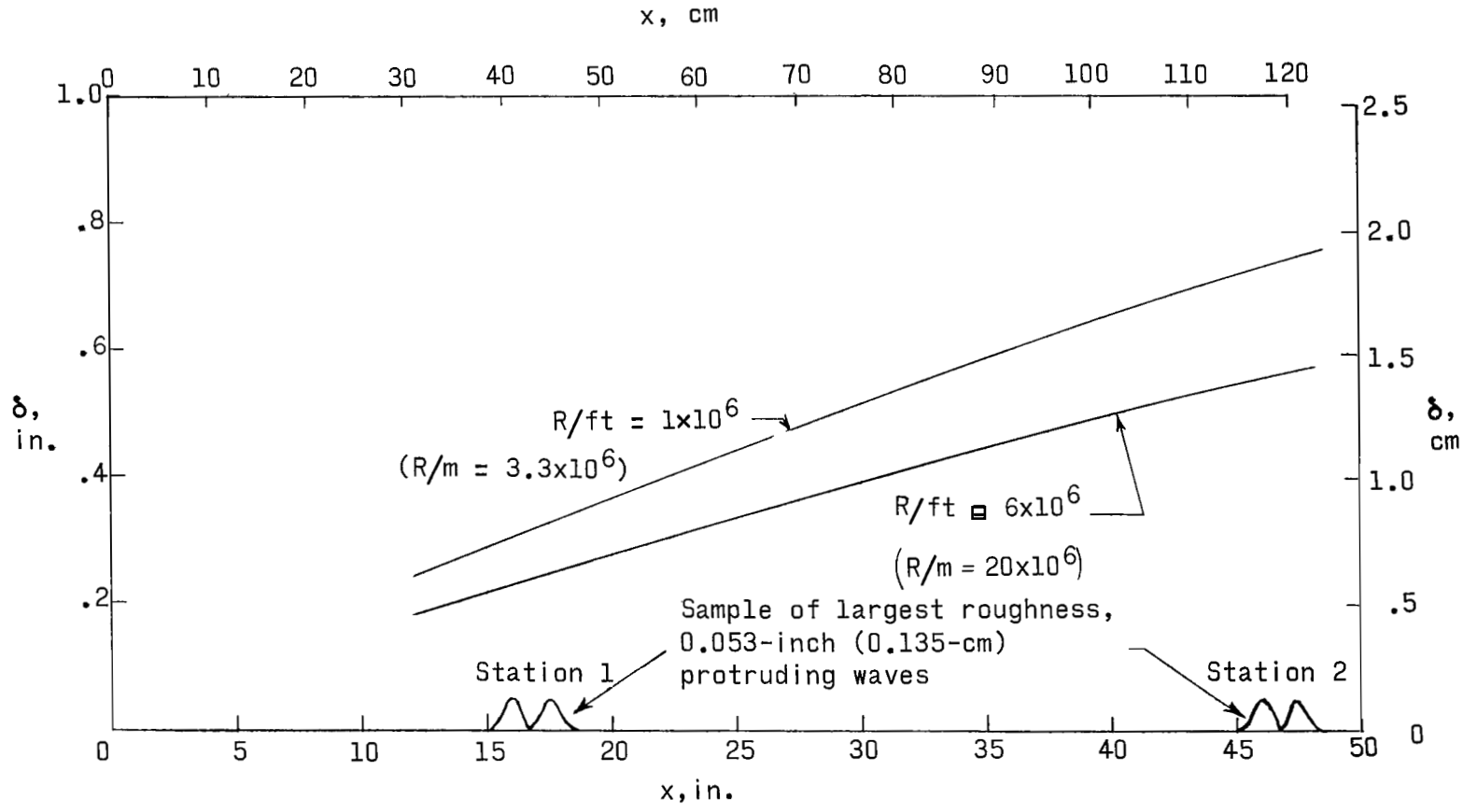

Figure 4.- Comparison of estimated total boundary-layer thickness δ with largest roughness, 0.053-inch (0.135-cm) protruding waves. $M_\infty = 1.00$.

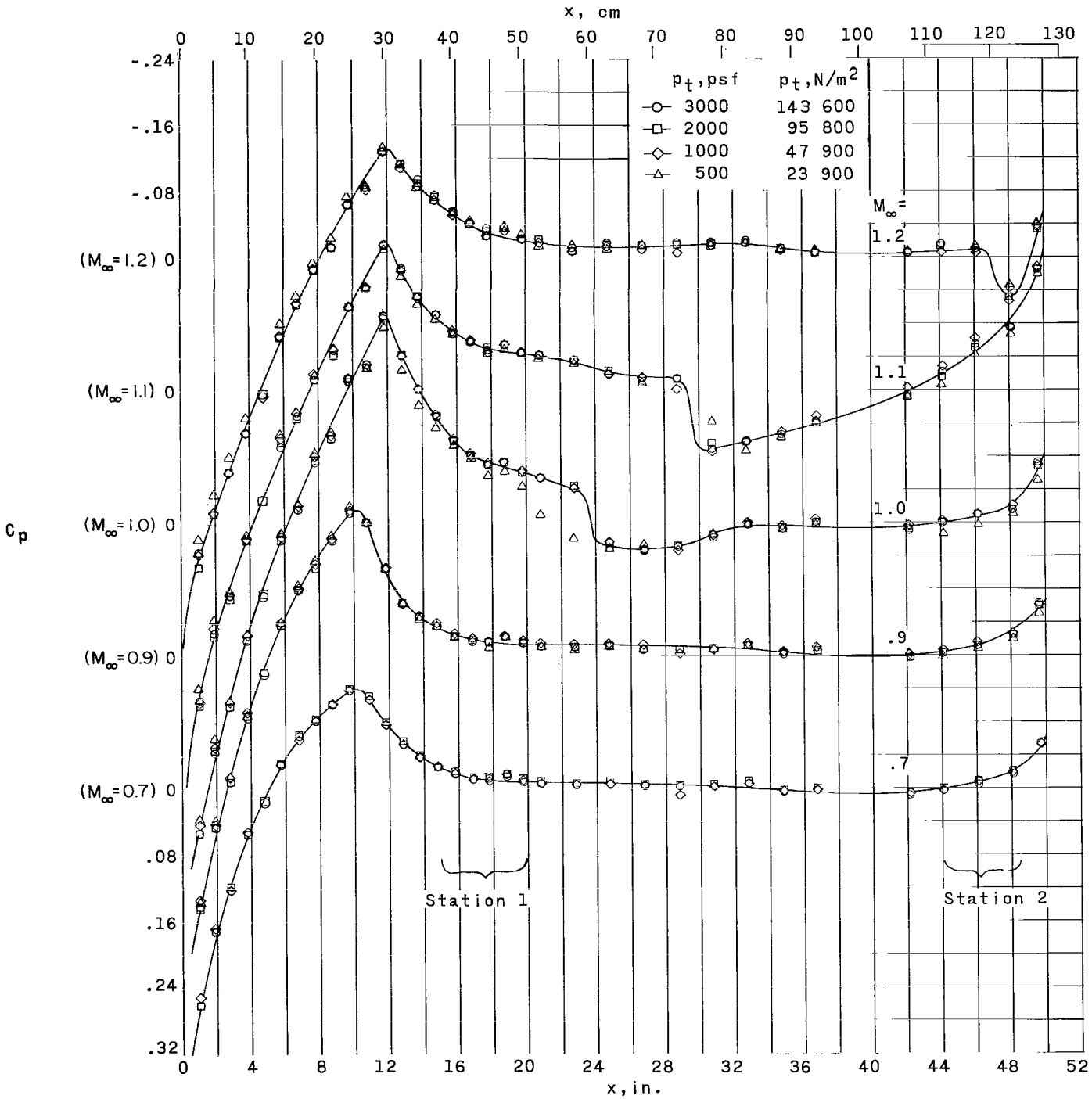

Figure 5.- Pressure distributions over basic smooth model.

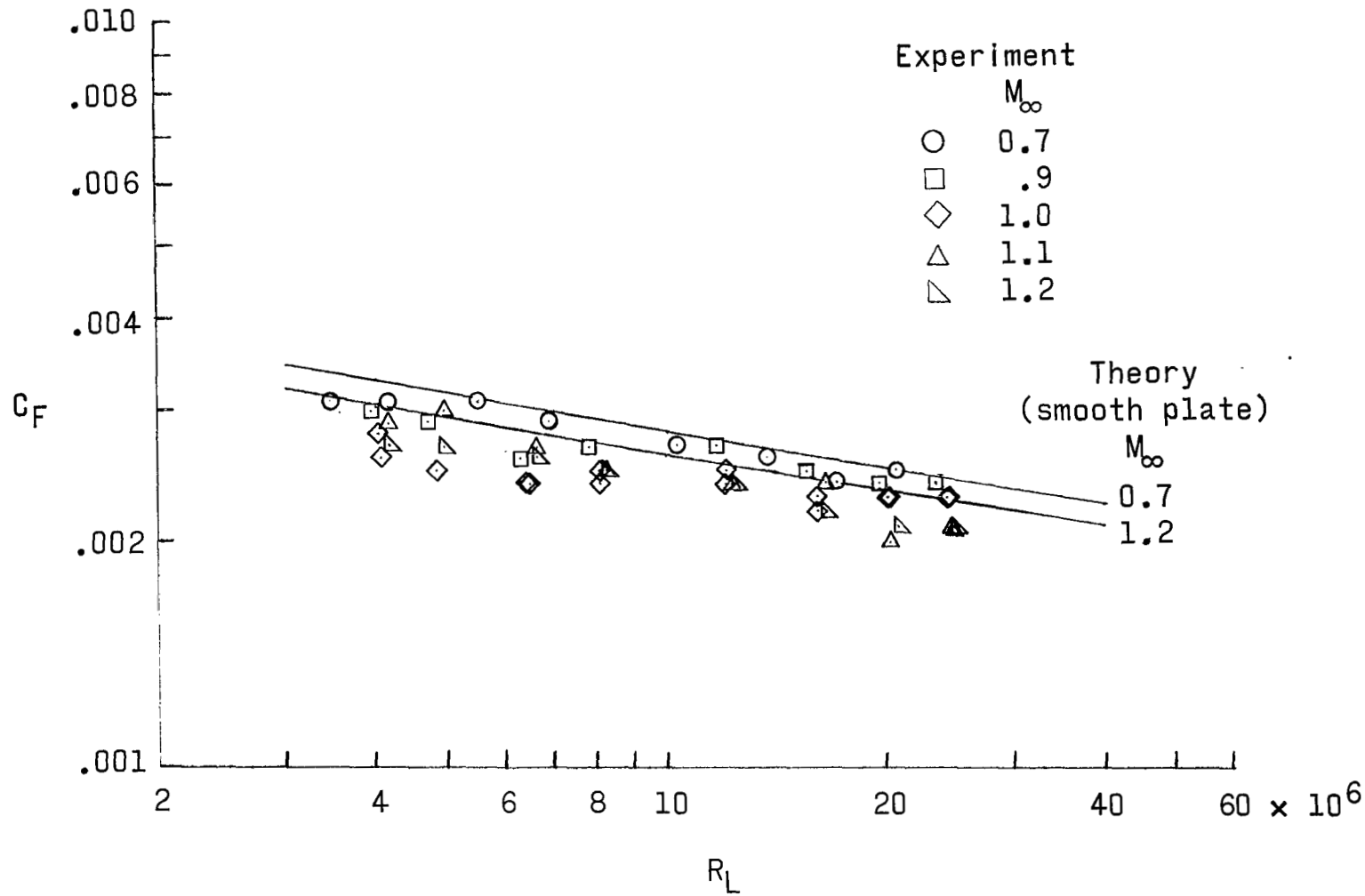

Figure 6.- Variation of skin-friction drag coefficient with Reynolds number. Model with smooth surface.

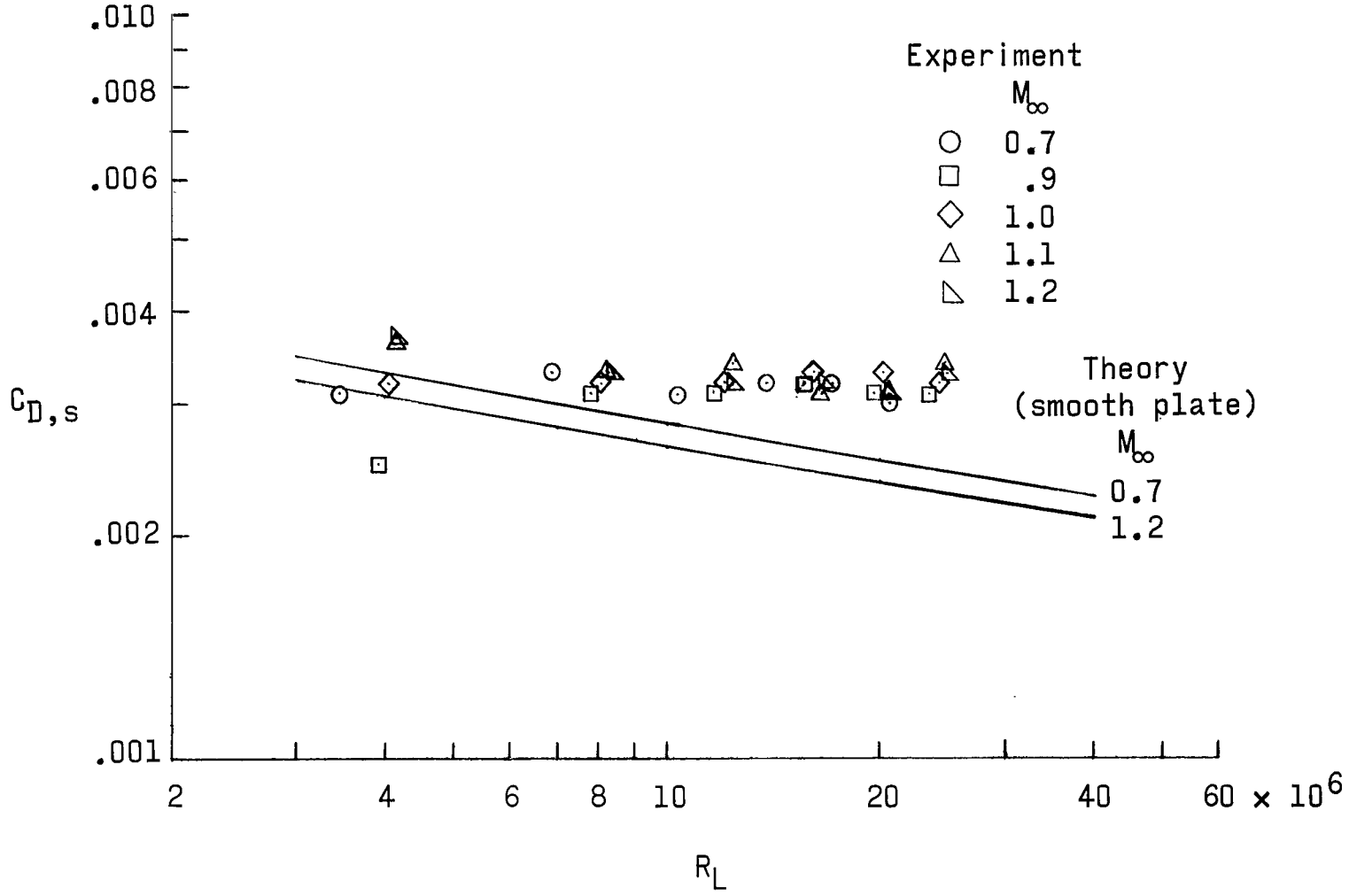

(a) 0.021-inch (0.053-cm) steps with grooves.

Figure 7.- Variation of surface-drag coefficient with Reynolds number for models with fabrication-type roughness. Flagged symbols indicate data obtained with larger drag beam.

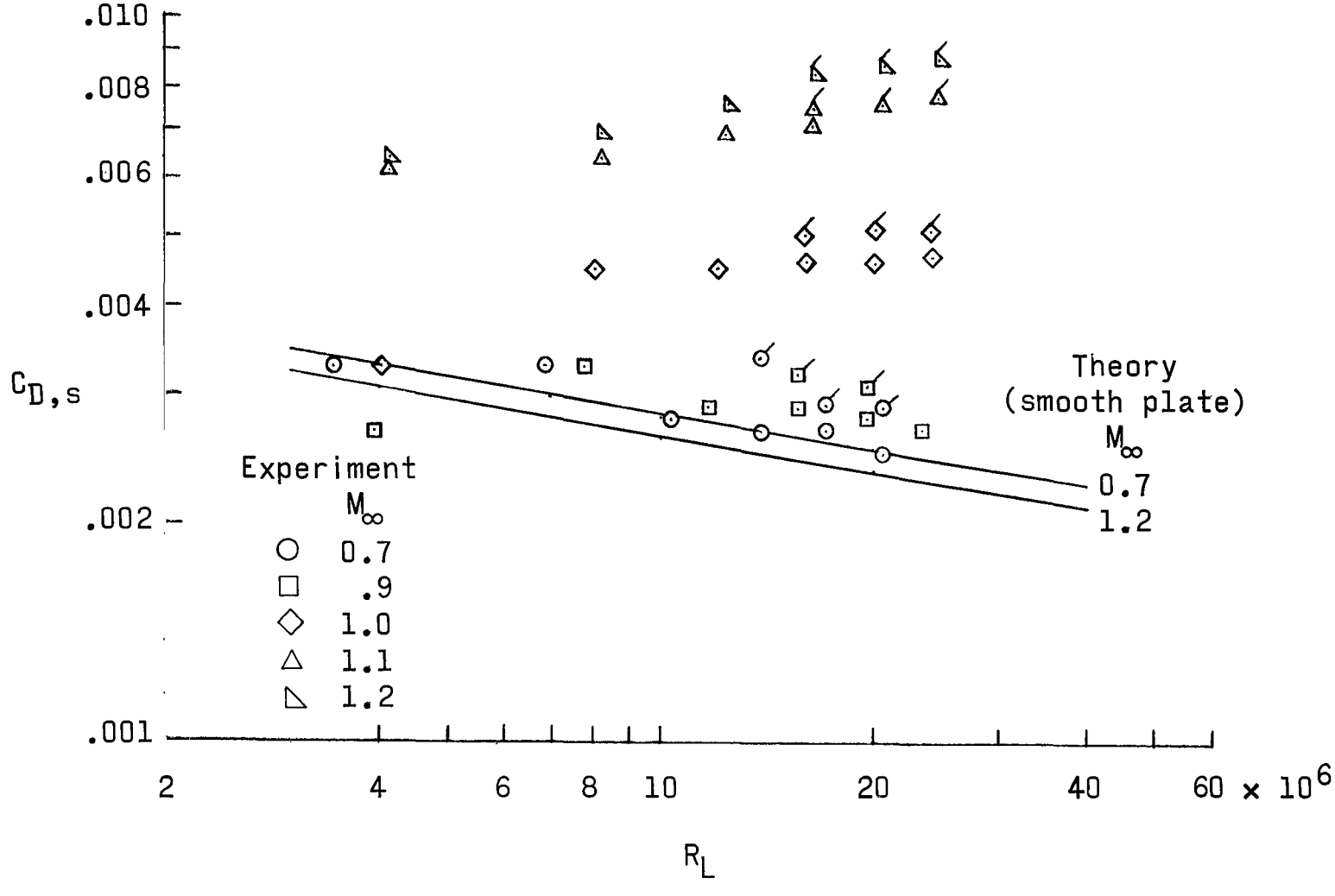

(b) 0.053-inch (0.135-cm) protruding waves.

Figure 7.- Continued.

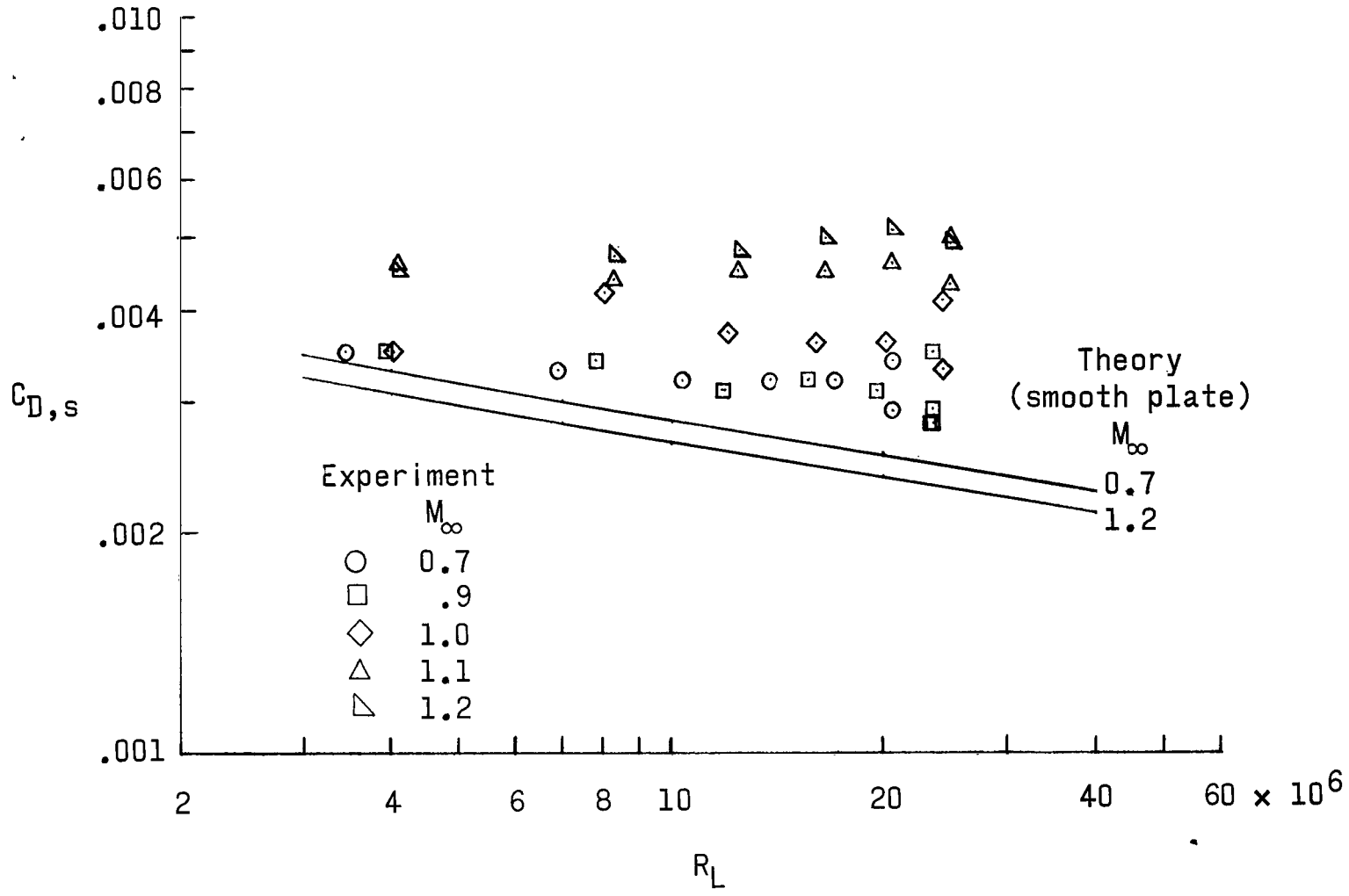

(c) 0.053-inch (0.135-cm) transverse creases.

Figure 7.- Continued.

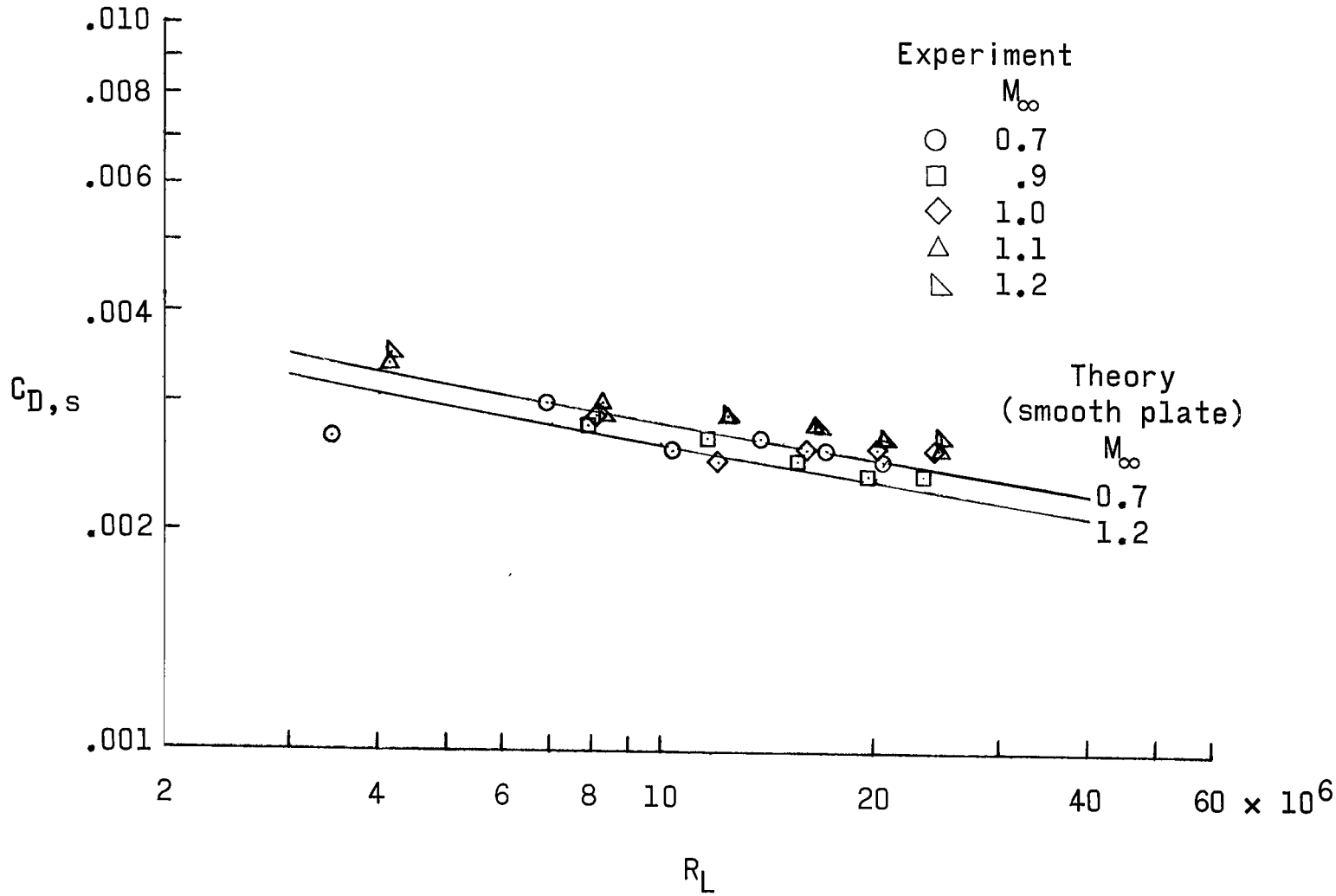

(d) 0.017-inch (0.043-cm) transverse creases.

Figure 7.- Continued.

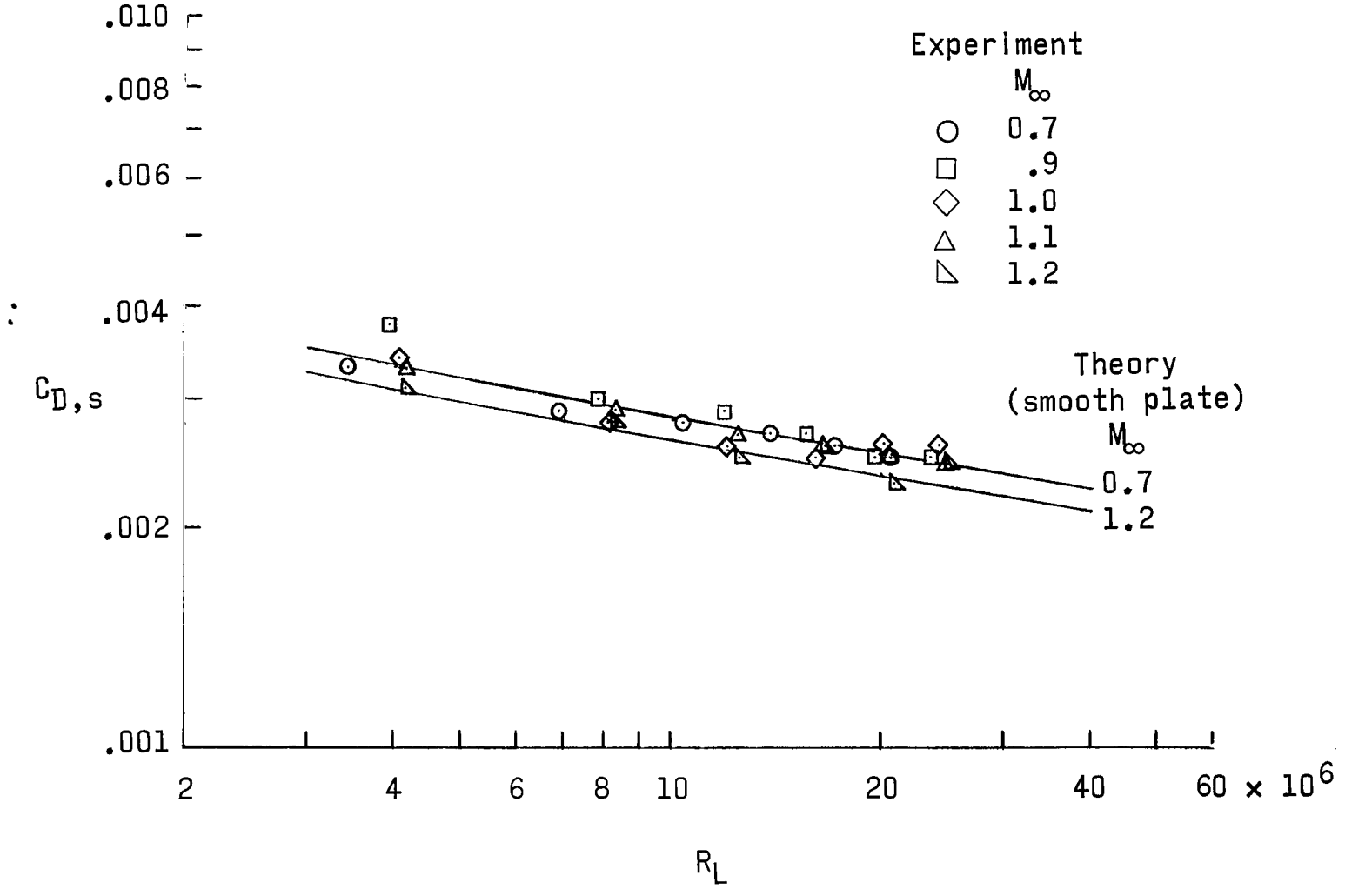

(e) 0.020-inch (0.051-cm) 45^0 rearward steps.

Figure 7.- Continued.

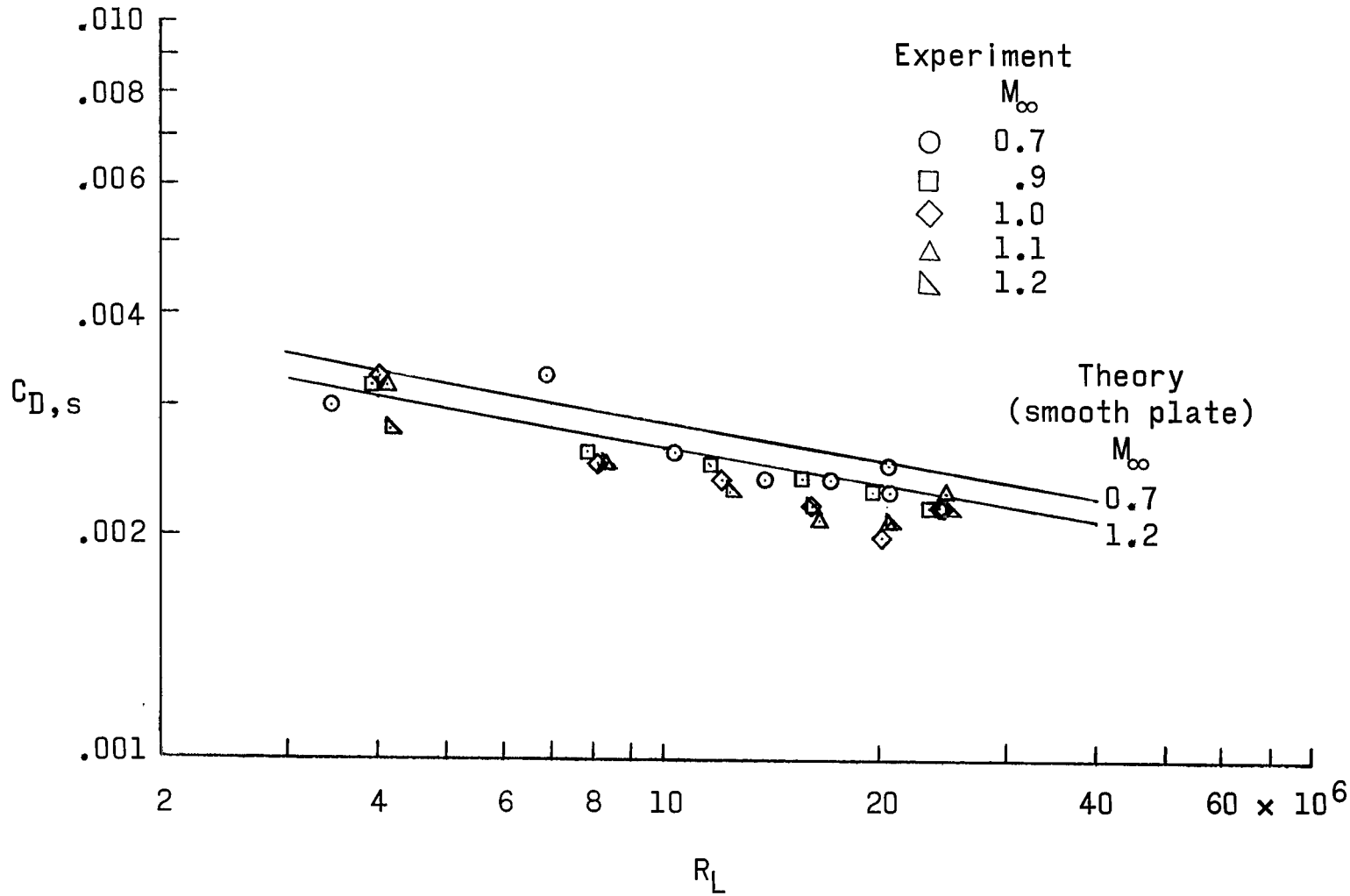

(f) 0.014-inch (0.036-cm) 45^0 creases.

Figure 7.- Concluded.

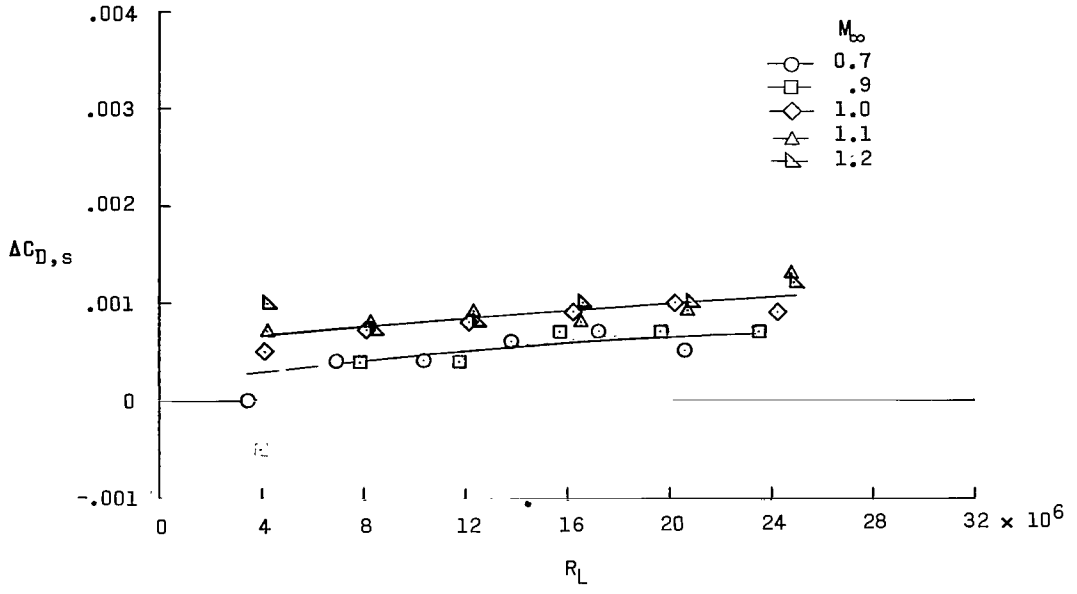

(a) 0.021-inch (0.053-cm) steps with grooves.

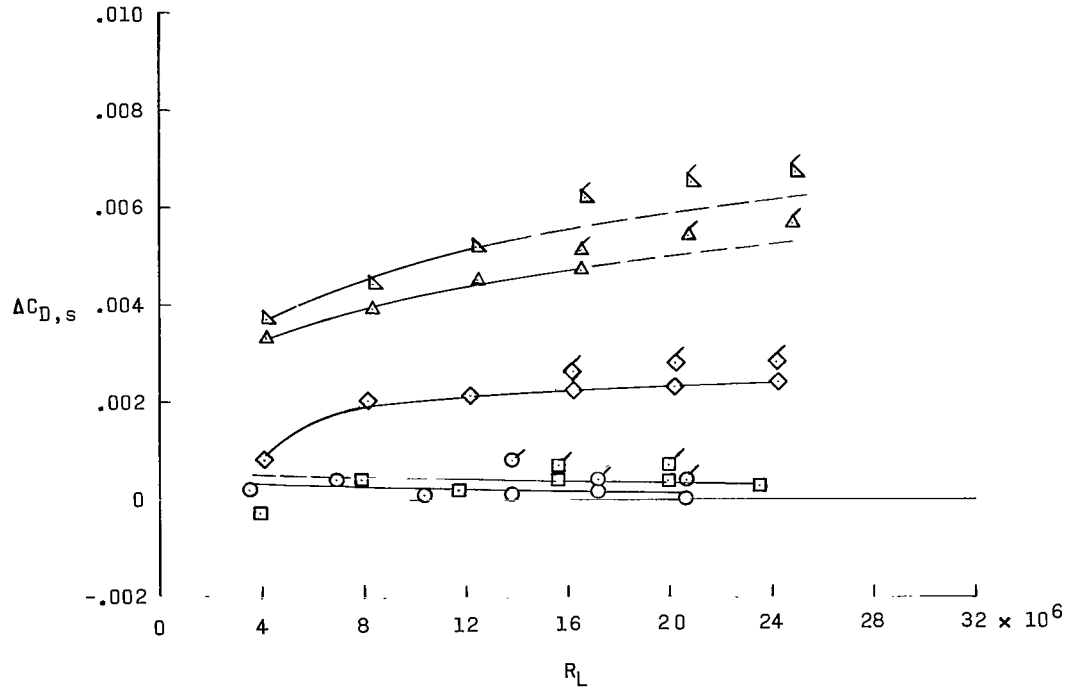

(b) 0.053-inch (0.135-cm) protruding waves.

Figure 8.- Variation of incremental surface-drag coefficient with Reynolds number and Mach number. Flagged symbols indicate data obtained with larger drag beam.

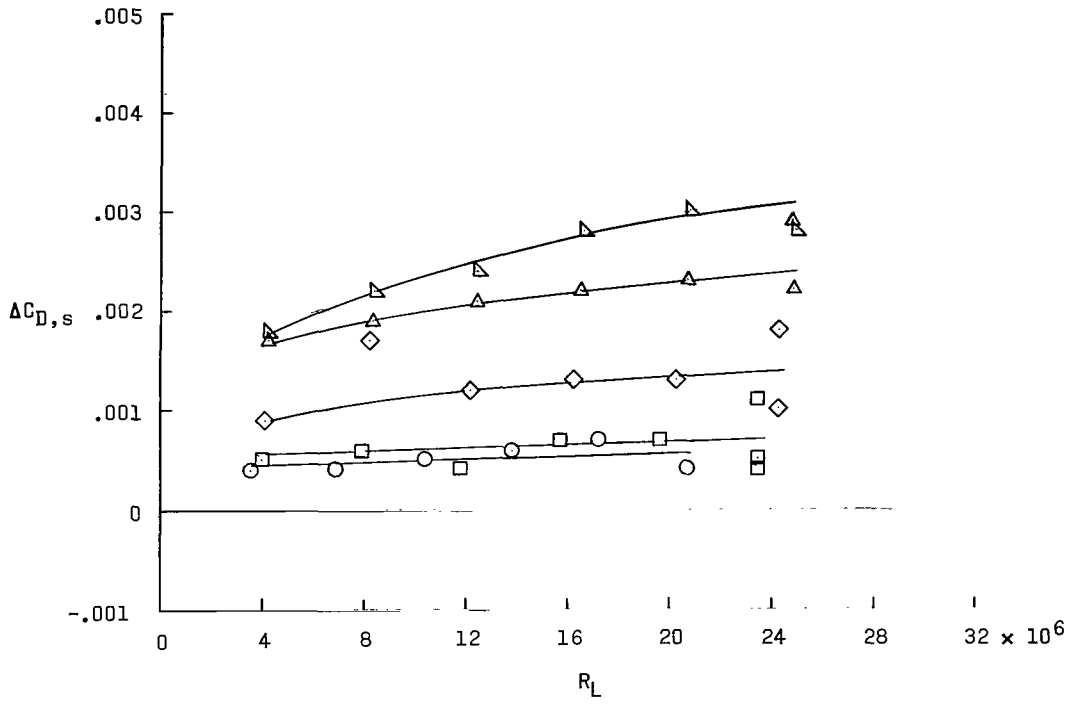

(c) 0.053-inch (0.135-cm) transverse creases.

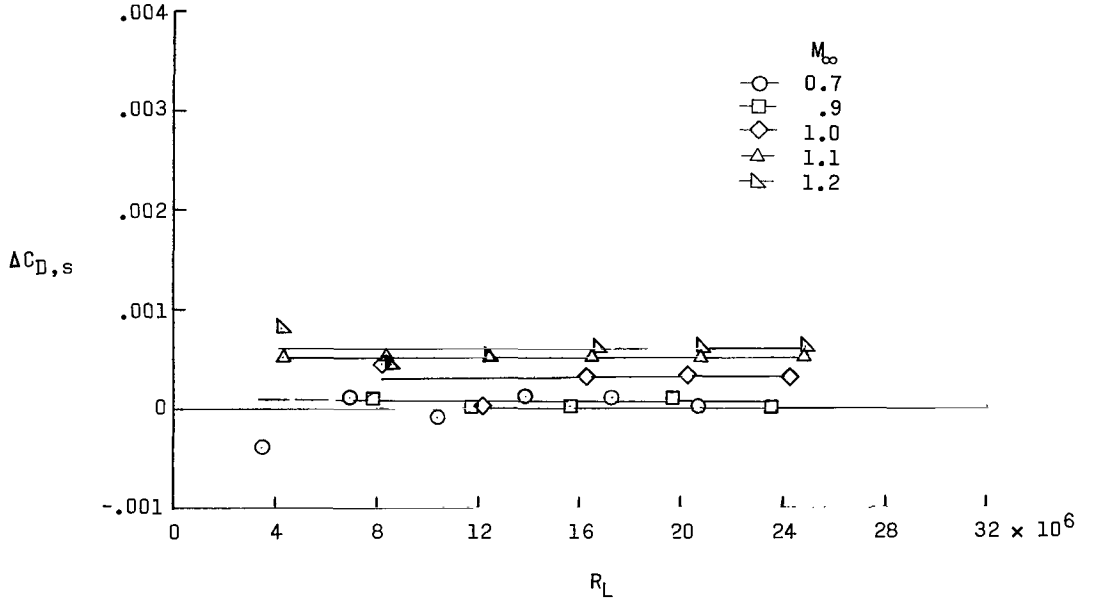

(d) 0.017-inch (0.043-cm) transverse creases.

Figure 8.- Continued.

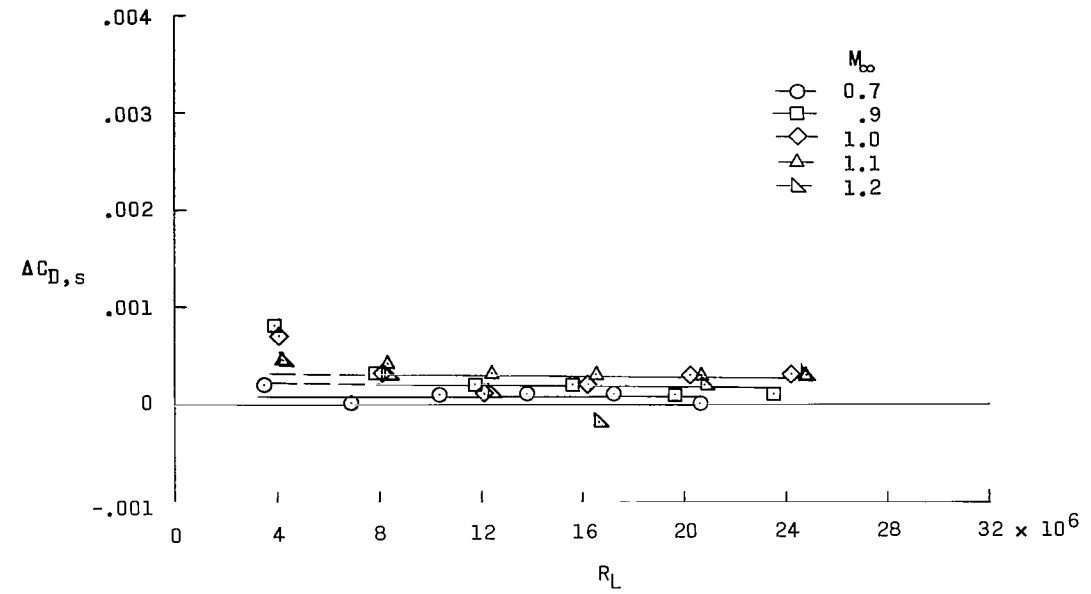

(e) 0.020-inch (0.051-cm) 45^0 rearward steps.

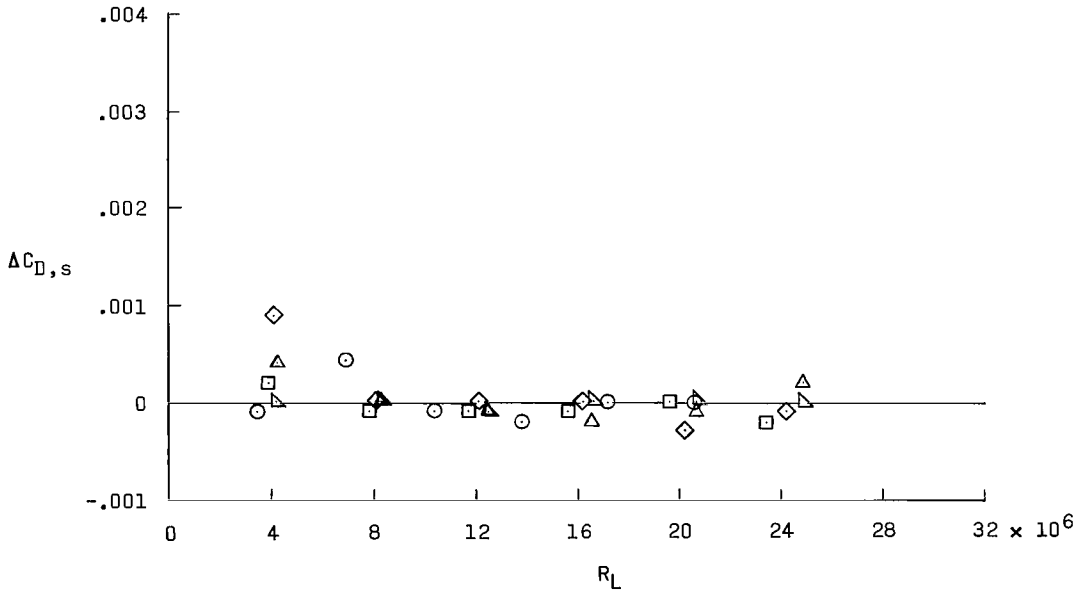

(f) 0.014-inch (0.036-cm) 45^0 rearward creases.

Figure 8.- Concluded.

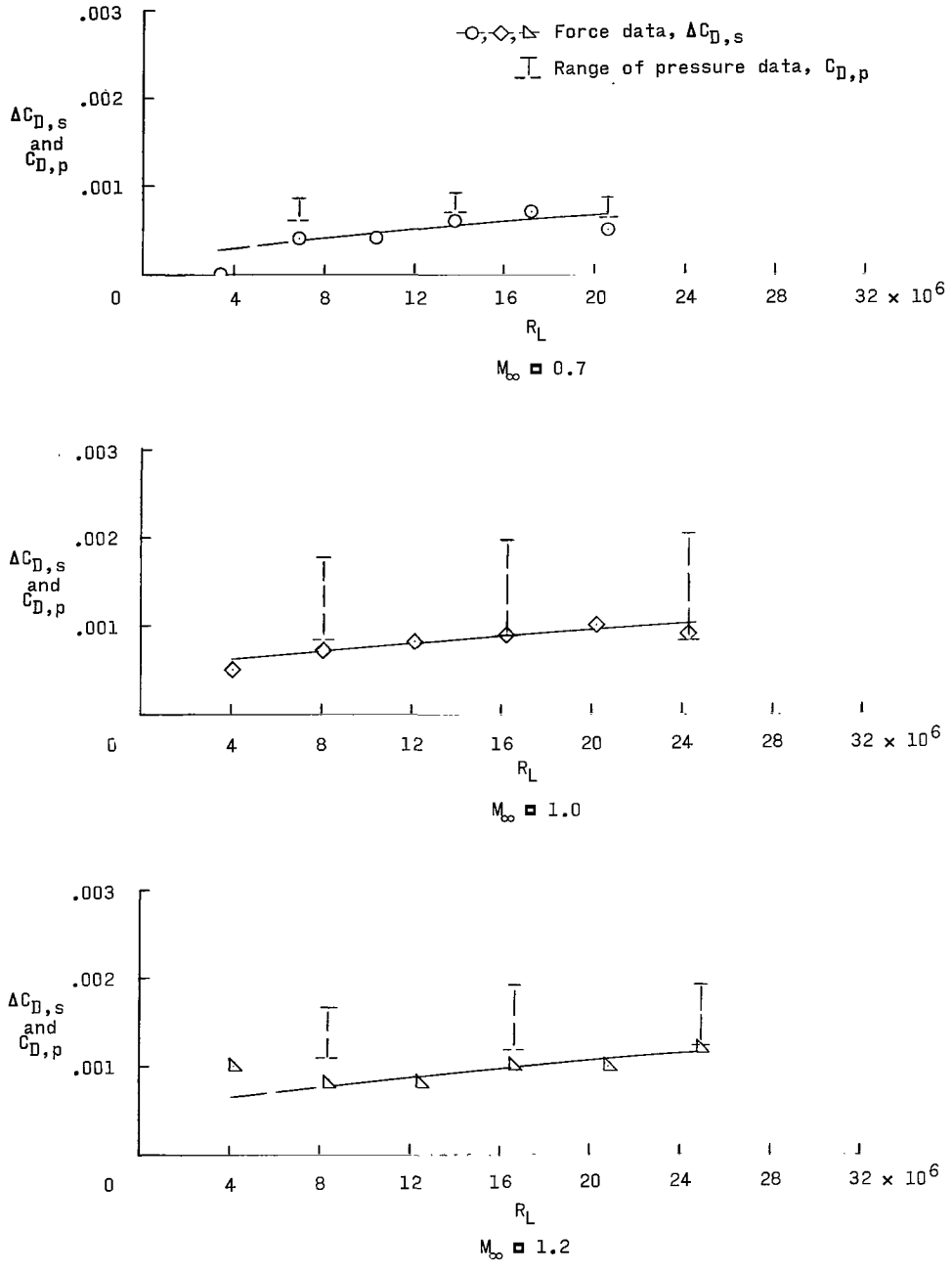

(a) 0.021-inch (0.053-cm) steps with grooves.

Figure 9.- Comparison of force-test data $\Delta C_{D,s}$ with pressure-drag results $C_{D,p}$, with Reynolds number as primary variable. Flagged symbols indicate data obtained with larger drag beam.

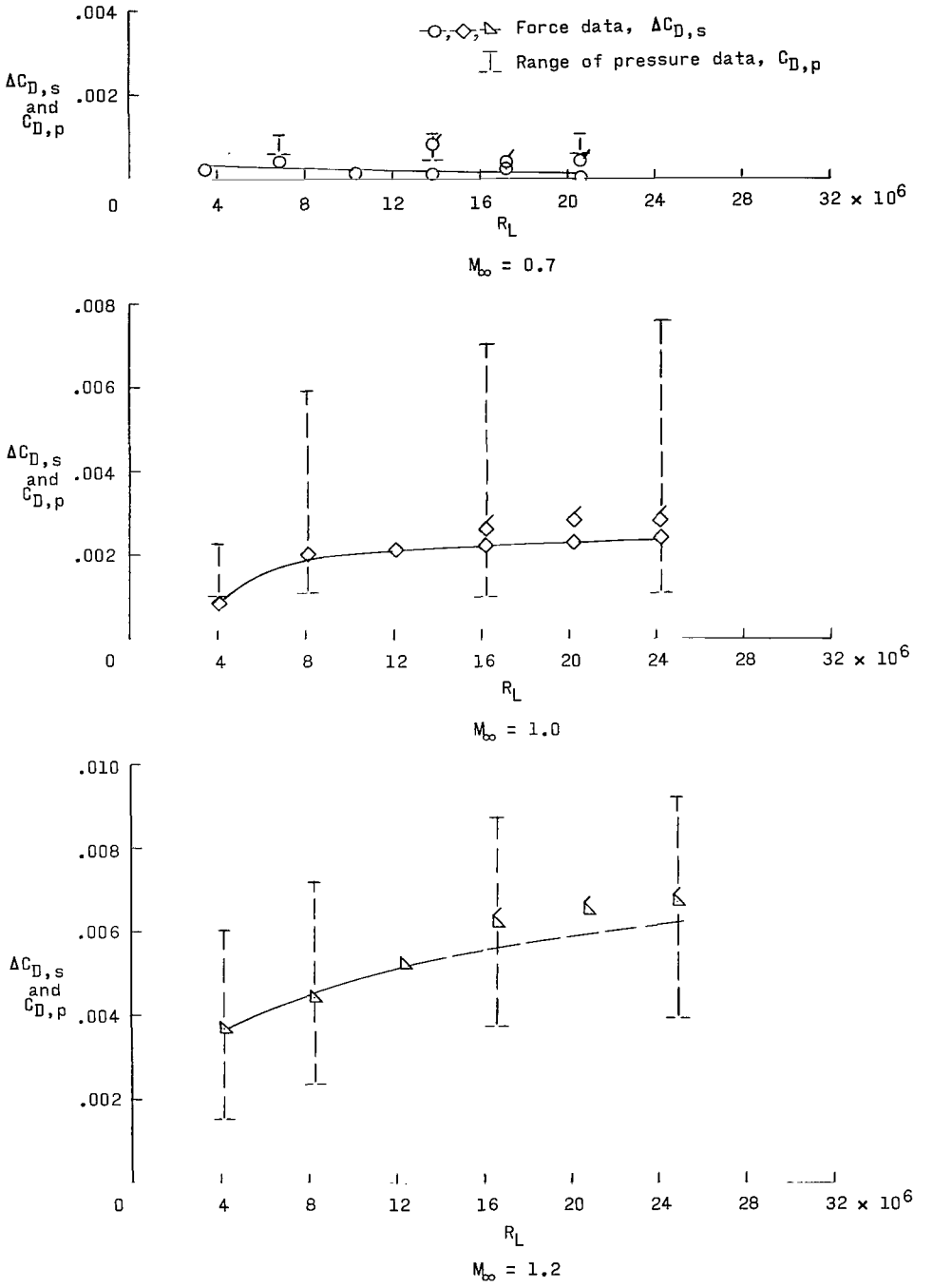

(b) 0.053-inch (0.135-cm) protruding waves.

Figure 9.- Continued.

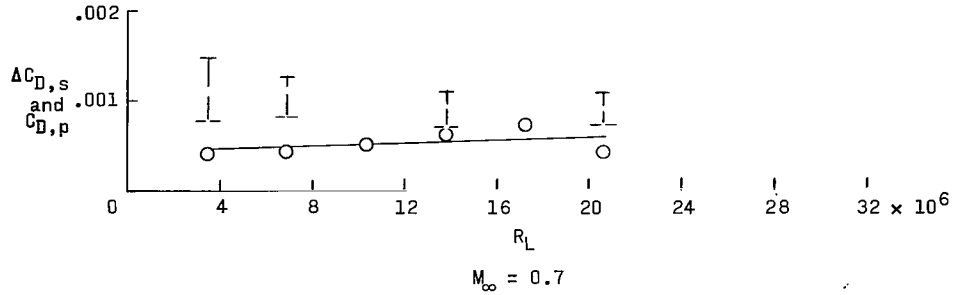

M_∞ = 0.7

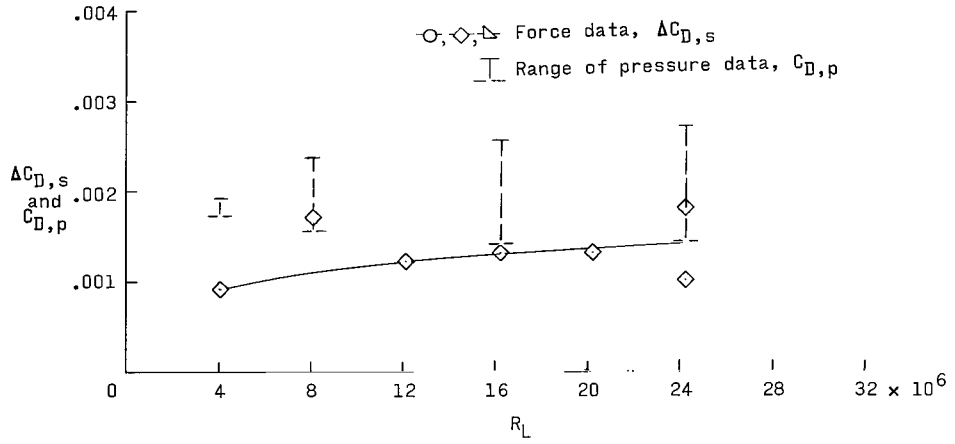

M_∞ = 1.0

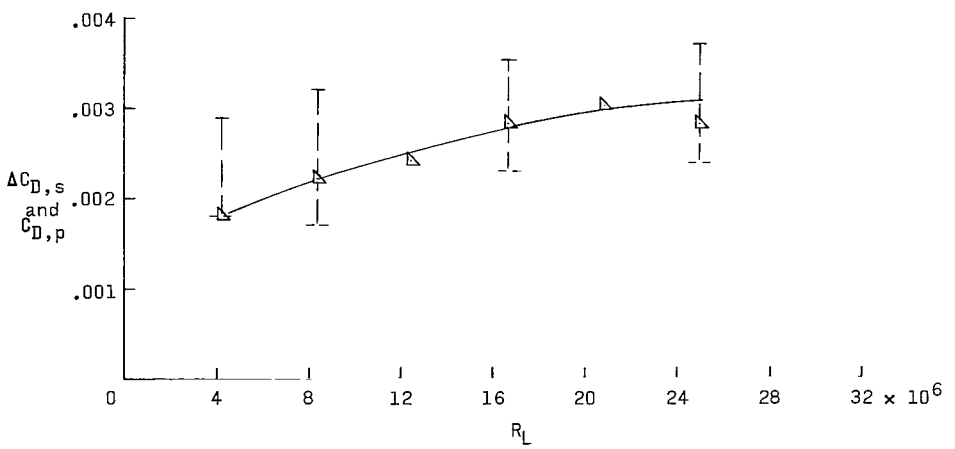

M_∞ ◘ 1.2

(c) 0.053-inch (0.135-cm) transverse creases.

Figure 9.- Continued.

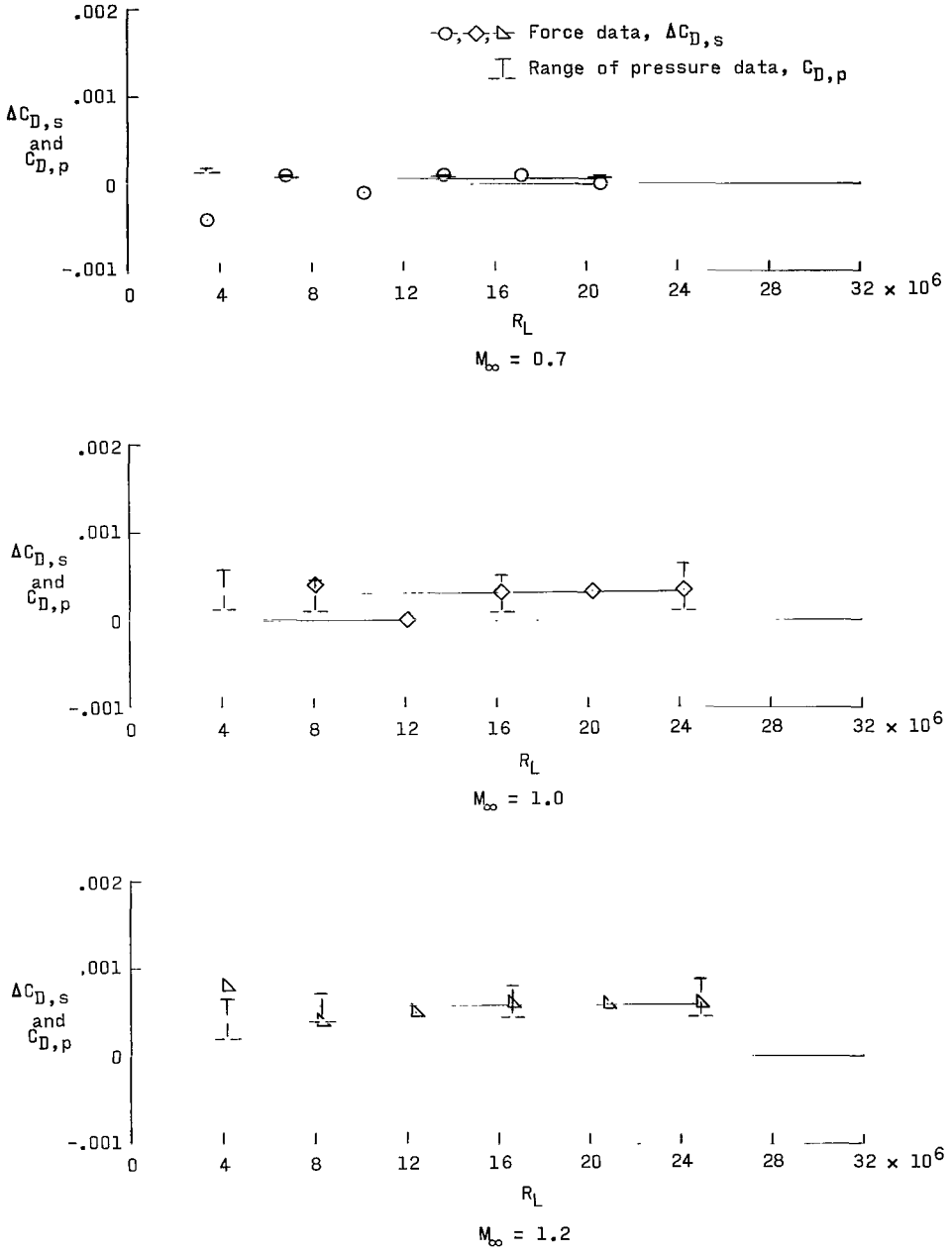

(d) 0.017-inch (0.043-cm) transverse creases.

Figure 9.- Continued.

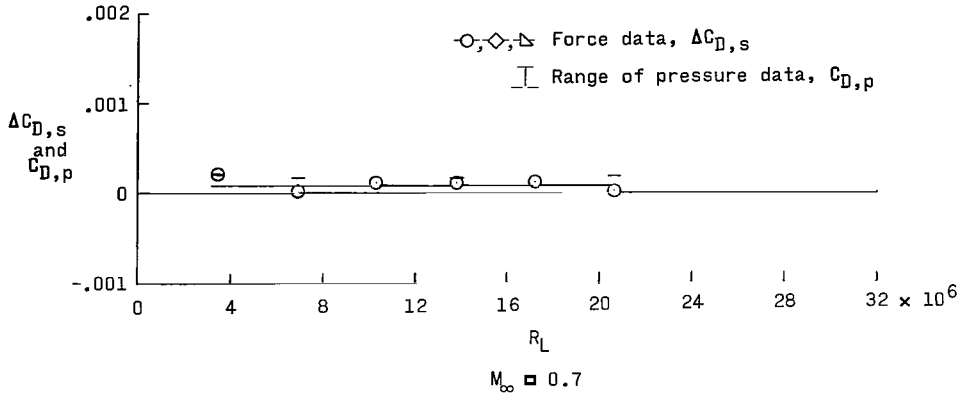

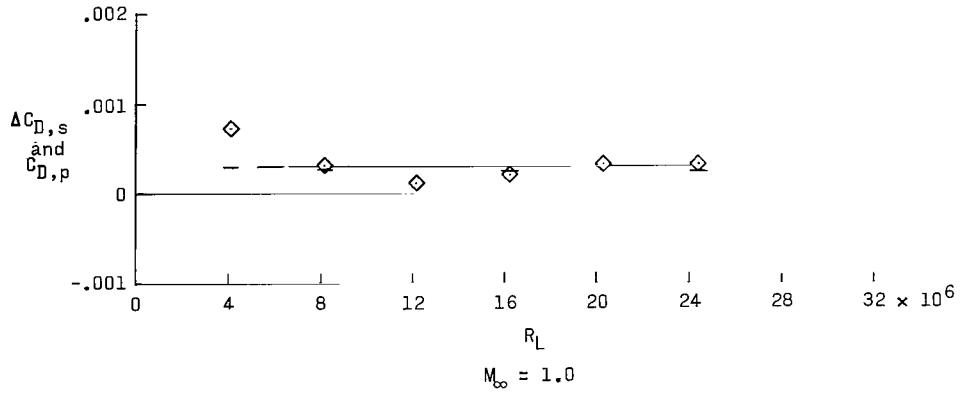

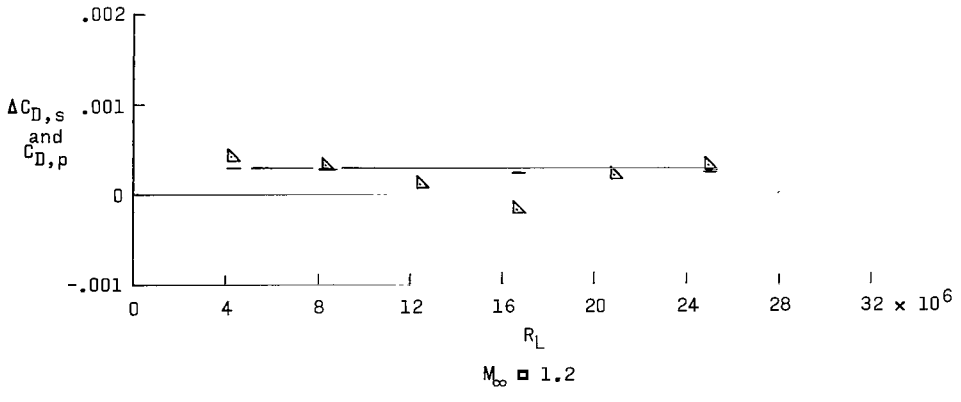

(e) 0.020-inch (0.051-cm) 45° rearward steps.

Figure 9.- Continued.

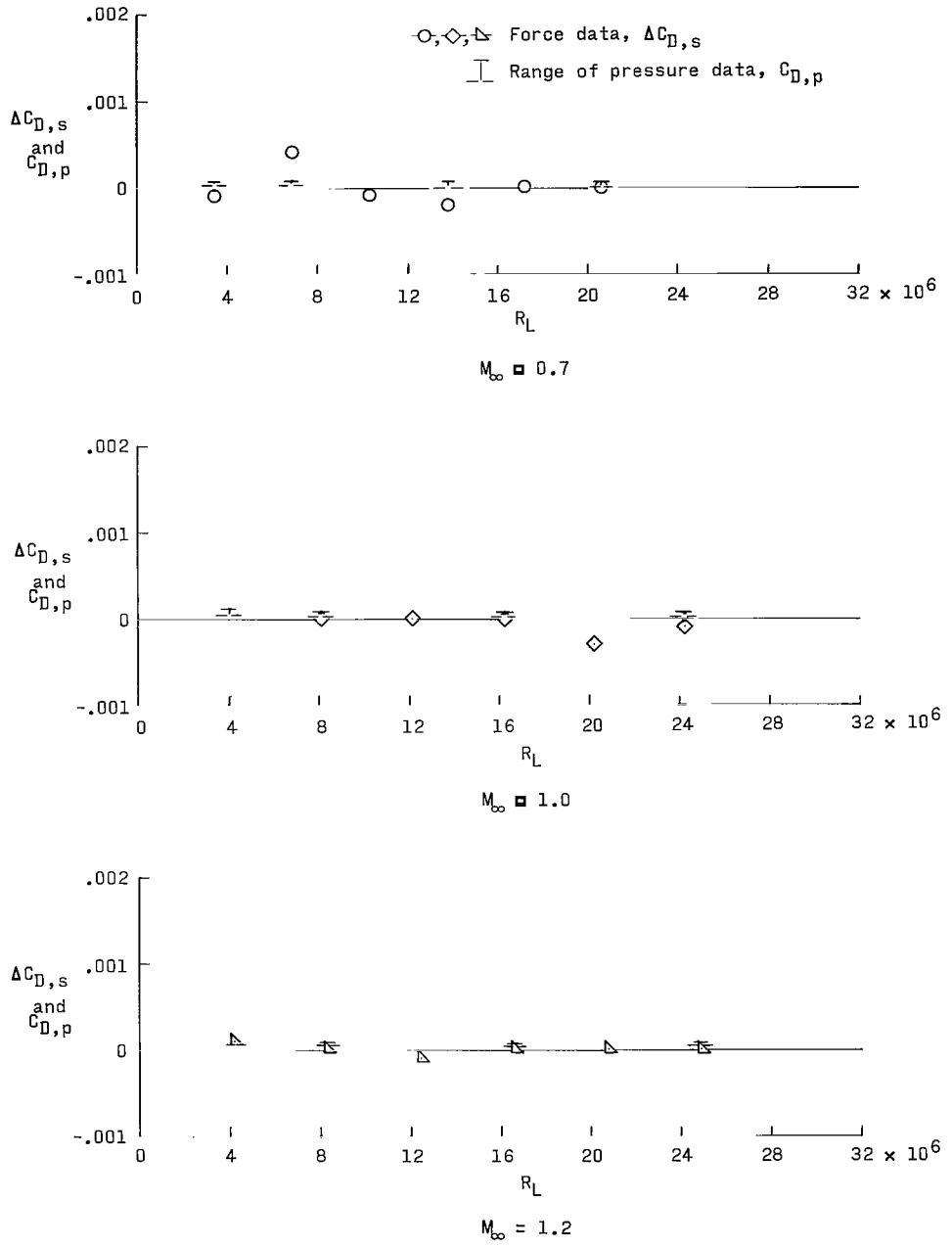

(f) 0.014-inch (0.036-cm) 45° creases.

Figure 9.- Concluded.

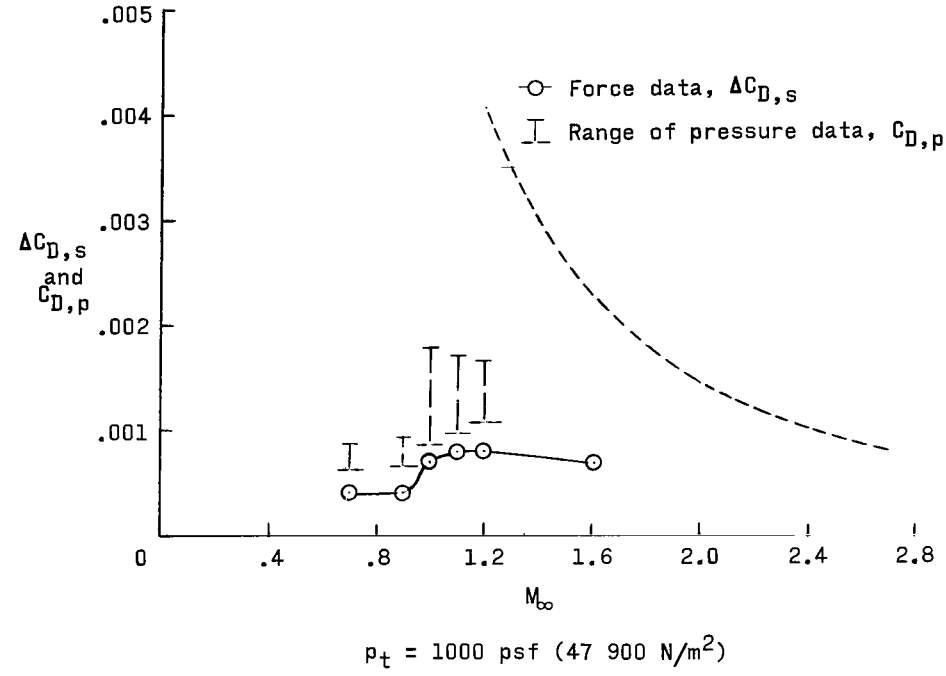

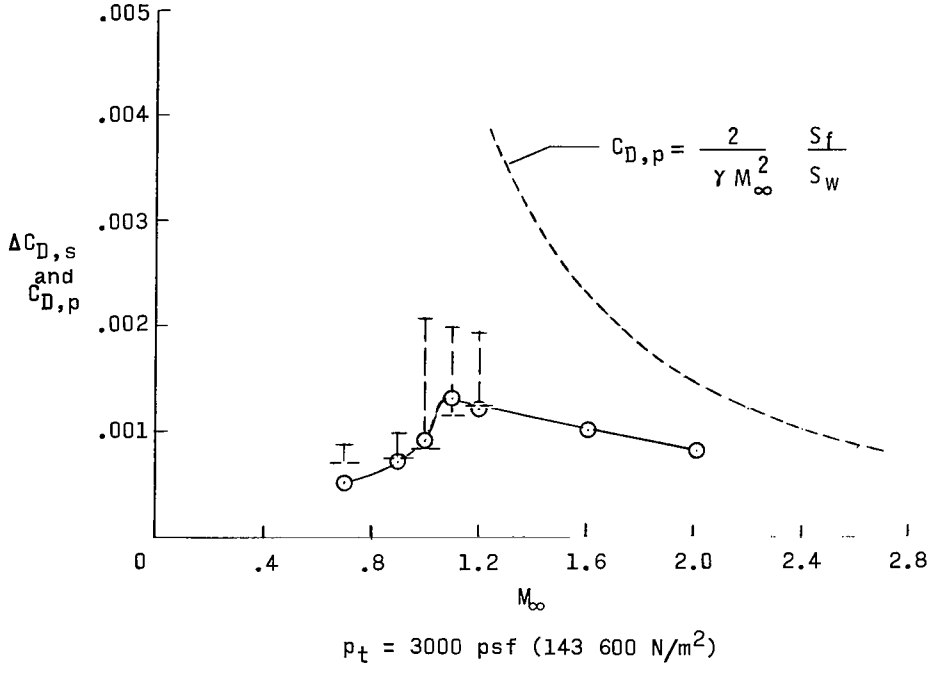

(a) 0.021-inch (0.053-cm) steps with grooves.

Figure 10.- Comparison of force-test data $\Delta C_{D,s}$ with pressure-drag results $C_{D,p}$, with Mach number as primary variable.

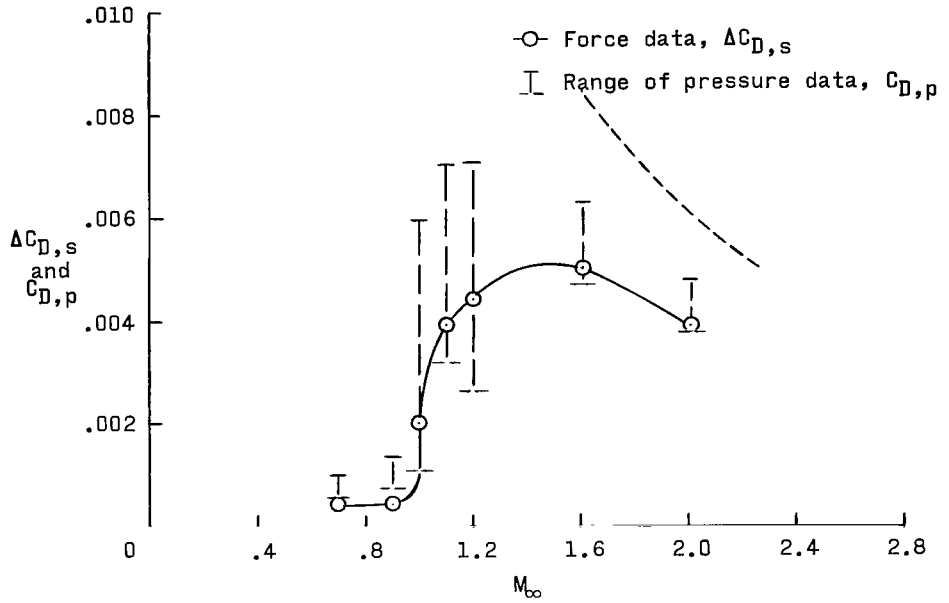

p_t = 1000 psf (47 900 N/m^2)

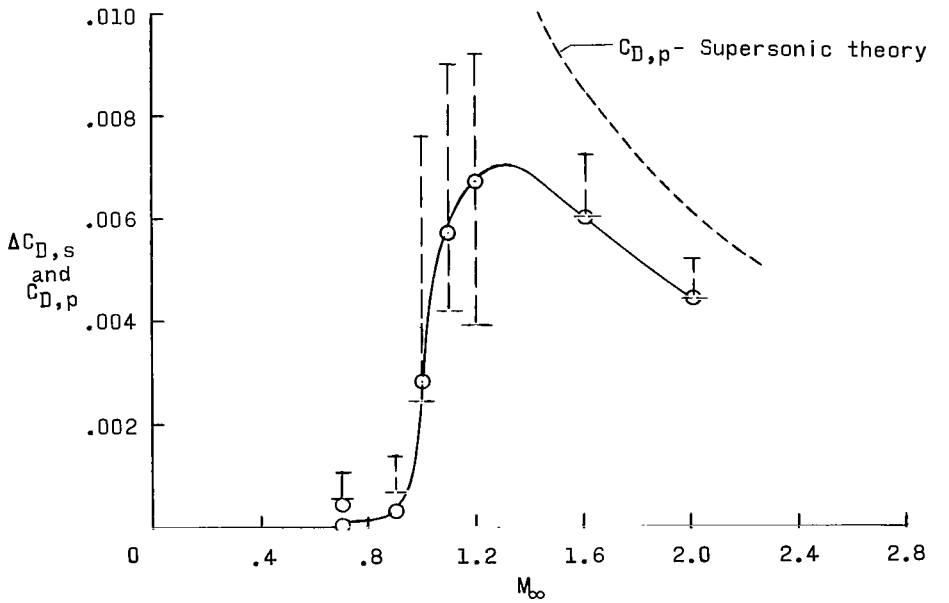

p_t = 3000 psf (143 600 N/m^2)

(b) 0.053-inch (0.135-cm) protruding waves.

Figure 10.- Continued.

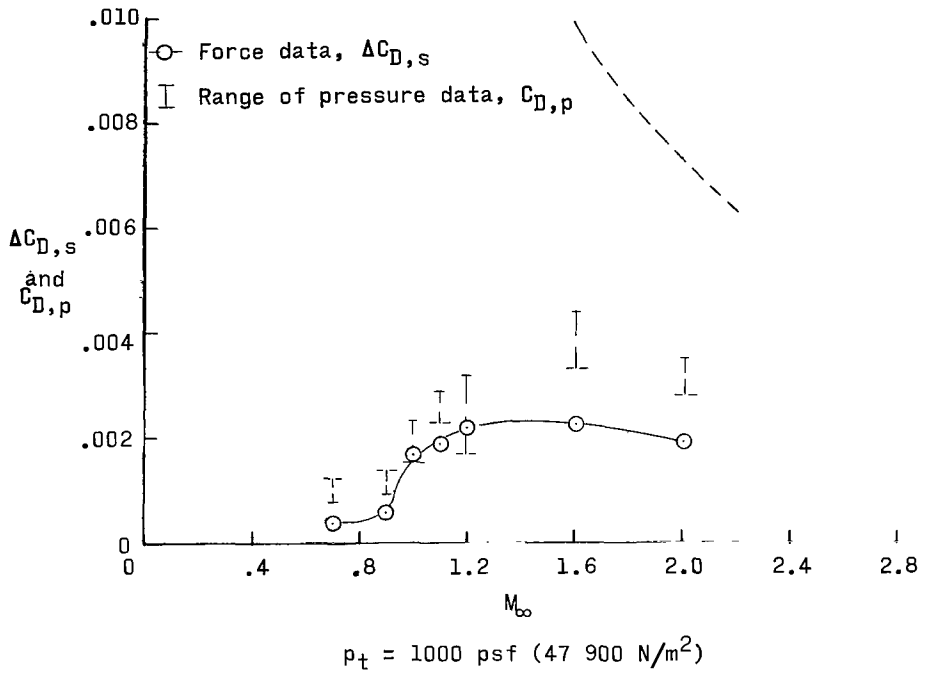

p_t = 1000 psf (47 900 N/m^2)

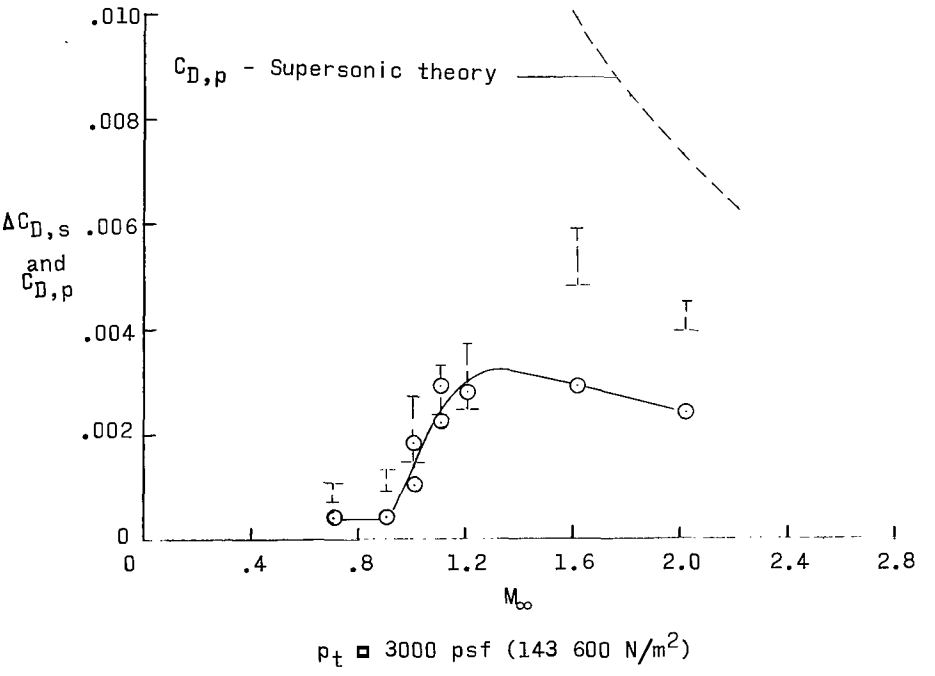

p_t ◻ 3000 psf (143 600 N/m^2)

(c) 0.053-inch (0.135-cm) transverse creases.

Figure 10.- Continued.

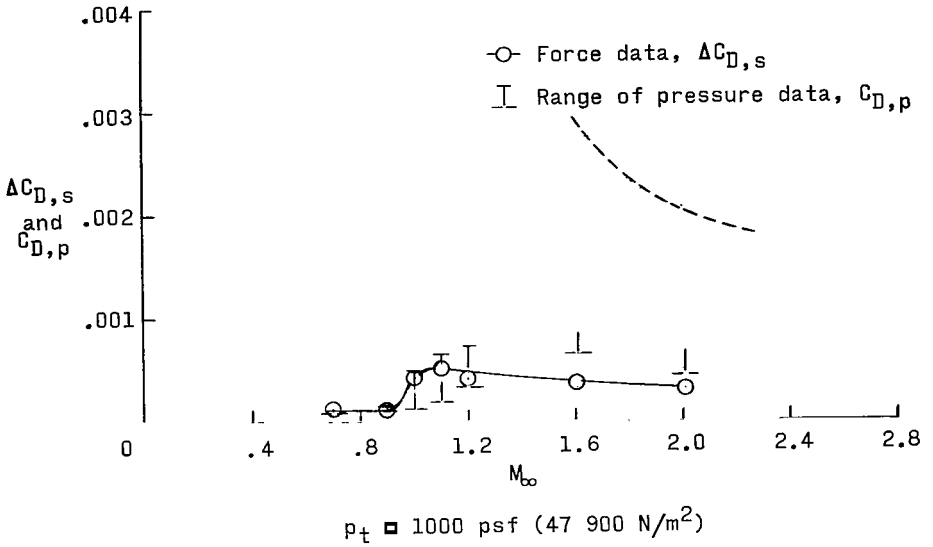

p_t ▫ 1000 psf (47 900 N/m^2)

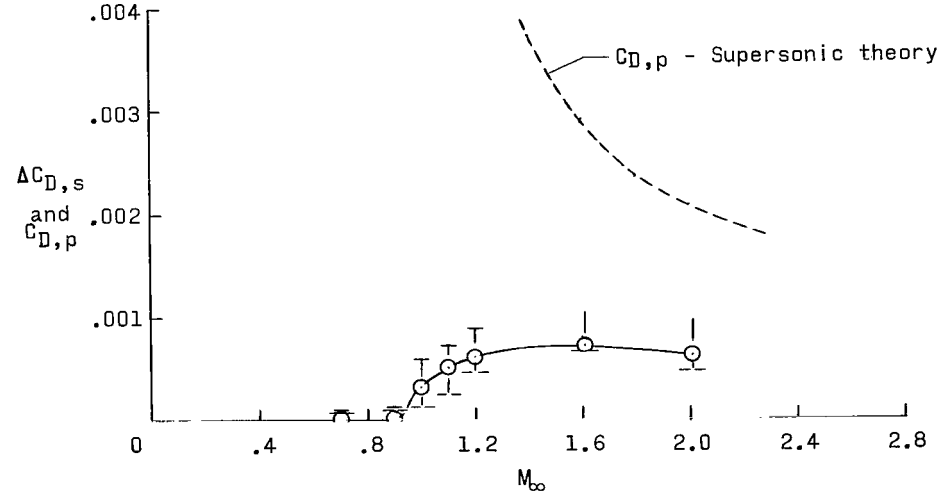

p_t = 3000 psf (143 600 N/m^2)

(d) 0.017-inch (0.043-cm) transverse creases.

Figure 10.- Continued.

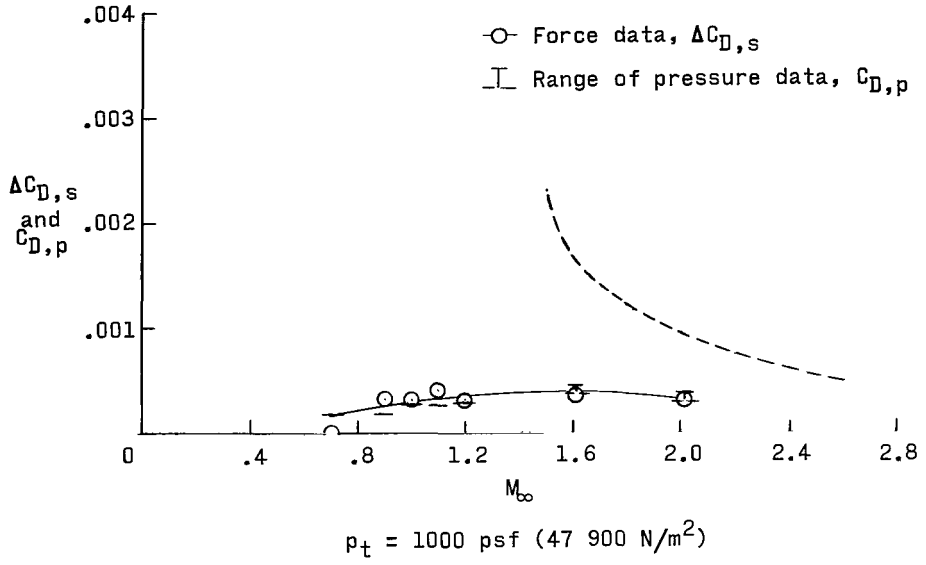

p_t = 1000 psf (47 900 N/m^2)

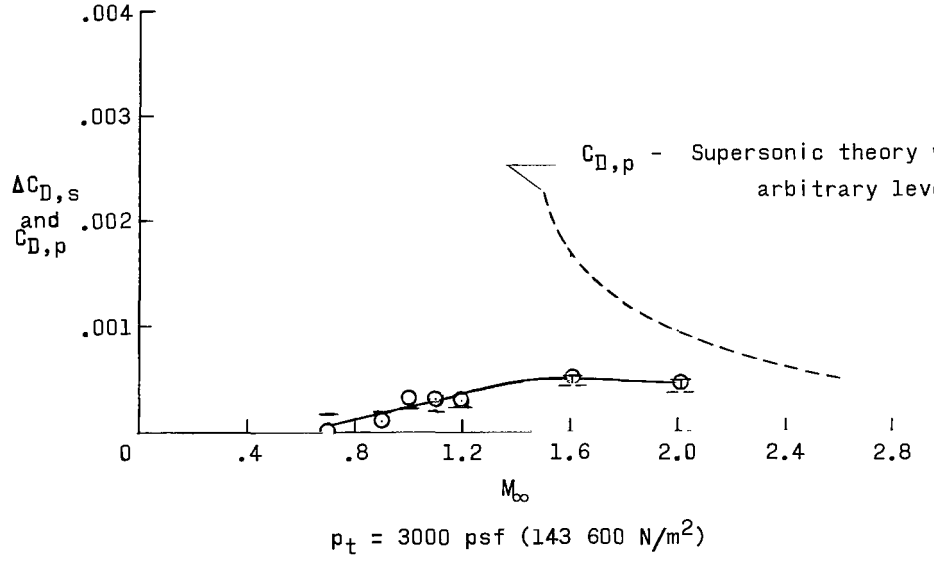

p_t = 3000 psf (143 600 N/m^2)

(e) 0.020-inch (0.051-cm) 45^0 rearward steps.

Figure 10.- Continued.

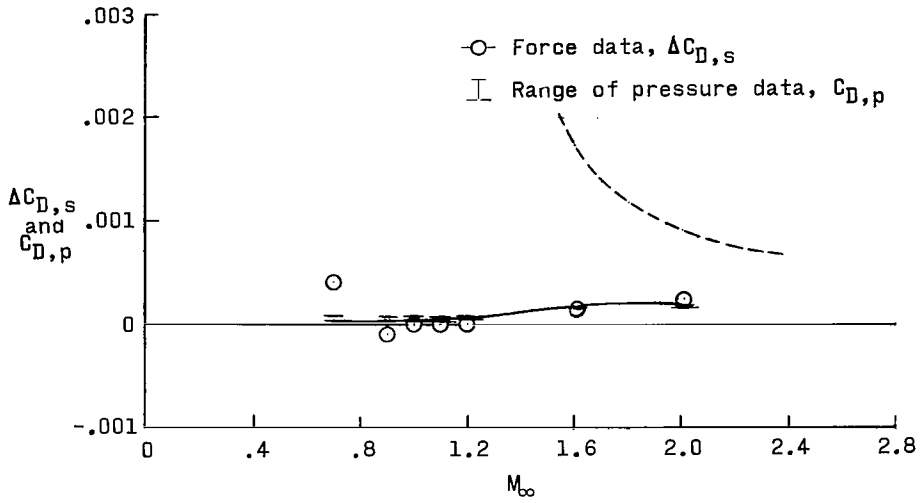

p_t = 1000 psf (47 900 N/m^2)

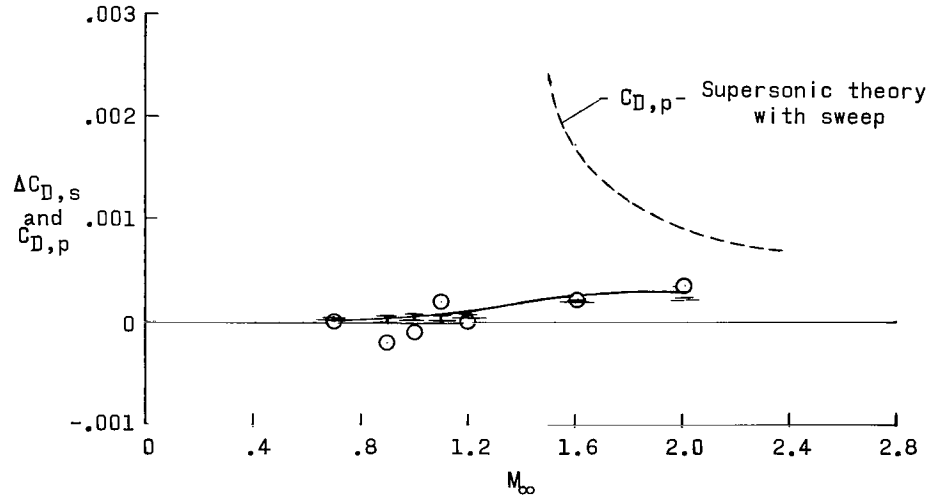

p_t = 3000 psf (143 600 N/m^2)

(f) 0.014-inch (0.036-cm) 45^0 creases.

Figure 10.- Concluded.